

Journal Pre-proof

Estimating surface temperature from thermal imagery of buildings for accurate thermal transmittance (U-value): A machine learning perspective

Debanjan Sadhukhan, Sai Peri, Niroop Sugunaraj, Avhishek Biswas, Daisy Flora Selvaraj, Katelyn Koiner, Andrew Rosener, Matt Dunlevy, Neena Goveas, David Flynn, Prakash Ranganathan



PII: S2352-7102(19)32726-3

DOI: <https://doi.org/10.1016/j.jobe.2020.101637>

Reference: JOBE 101637

To appear in: *Journal of Building Engineering*

Received Date: 3 December 2019

Revised Date: 27 June 2020

Accepted Date: 30 June 2020

Please cite this article as: D. Sadhukhan, S. Peri, N. Sugunaraj, A. Biswas, D.F. Selvaraj, K. Koiner, A. Rosener, M. Dunlevy, N. Goveas, D. Flynn, P. Ranganathan, Estimating surface temperature from thermal imagery of buildings for accurate thermal transmittance (U-value): A machine learning perspective, *Journal of Building Engineering* (2020), doi: <https://doi.org/10.1016/j.jobe.2020.101637>.

This is a PDF file of an article that has undergone enhancements after acceptance, such as the addition of a cover page and metadata, and formatting for readability, but it is not yet the definitive version of record. This version will undergo additional copyediting, typesetting and review before it is published in its final form, but we are providing this version to give early visibility of the article. Please note that, during the production process, errors may be discovered which could affect the content, and all legal disclaimers that apply to the journal pertain.

© 2020 Published by Elsevier Ltd.

Authors Statement:

Debanjan Sadhukhan (Writing - Original Draft, Methodology, Software, Data Curation, Visualization, Validation, Writing - Review & Editing)

Sai Peri (Software, Writing, Data Curation, Visualization, Investigation)

Niroop Sugunaraj (Software, Data Curation, Visualization, Investigation, Writing - Review & Editing)

Avhishek Biswas (Software, Data Curation, Visualization)

Daisy Flora Selvaraj (Writing - Review & Editing, Methodology)

Katelyn Koiner (Software, Methodology, Writing - Review & Editing, Writing - Original Draft)

Andrew Rosener (Software, Methodology, Writing - Review & Editing, Writing - Original Draft)

Matt Dunlevy (Resources)

Neena Goveas (Writing - Review & Editing)

David Flynn (Conceptualization, Writing - Review & Editing)

Prakash Ranganathan (Conceptualization, Methodology, Supervision, Project administration, Funding acquisition, Writing - Review & Editing, Resources, Formal Analysis)

Estimating Surface Temperature from Thermal Imagery of Buildings for Accurate Thermal Transmittance (U-value): A Machine Learning Perspective

Debanjan Sadhukhan^a, Sai Peri^a, Niroop Sugunaraj^a, Avhishek Biswas^a, Daisy Flora Selvaraj^a, Katelyn Koiner^a, Andrew Rosener^a, Matt Dunlevy^b, Neena Goveas^a, David Flynn^c, and Prakash Ranganathan^a

^aSchool of Electrical Engineering and Computer Science University of North Dakota, Grand Forks, ND, USA

^bSkySkopes Inc, Grand Forks, ND, USA

^cDepartment of Economics & Finance, University of North Dakota, Grand Forks, ND, USA

Abstract

Thermal performance assessment of building(s) is an essential process for optimal energy management, heat-loss evaluation, and energy audit applications. Such an assessment can help foresee the requirements for future intervention(s) and aid in benchmarking energy performance. This paper provides a review of several thermal performance assessment techniques and a broad classification based on measurement types, methods, and applications. Moreover, the article provides a comprehensive survey of various quantitative indices utilized for practical heat-loss assessment of building elements. This paper's unique contribution is the proposed three-layer framework that details the handling and processing of UAS-based thermal imagery for heat loss quantification. Primarily, the novelty of this work lies in the application of instance segmentation technique (e.g., Mask R-CNN) to compute the thermal transmittance values (e.g., U-values) for various objects (e.g., doors, walls, windows, and facades). To the best of our knowledge, this research work is first-of-its-kind using a sizeable thermal data repository (e.g. 100,000 augmented images). Multiple standard U-values are analyzed for windows and walls and compared with The American Society of Heating, Refrigerating, and Air-conditioning Engineers (ASHRAE) building standards. The preliminary results of Mask-RCNN from over 100,000 trained (including augmented) images from multiple campus buildings yield the following performance metrics: 1) provides an Average Precision (AP) of 0.67 (windows) and 0.46 (facades); and 2) Intersection of Union (IoU) of 0.05 (windows) and 0.5 (facades) respectively. Moreover, the U-values are consistently close enough to the ASHRAE standards in distinguishing window types (e.g. 0.77 for single-pane windows and 0.38 for double-pane windows).

Keywords

Infrared Thermography, Instance Segmentation, UAS, U-value.

1. Introduction

The energy management of a building is primarily driven by the heating or cooling requirements. Sustainable energy management in buildings requires minimization of heating or cooling loss. This loss often takes place across through various elements of the building such as walls, roofs or windows [1–3]. Assessing the thermal performance of these building elements is crucial for efficient energy management operations. These assessment techniques can be divided into qualitative and quantitative approaches.

Table 1. Nomenclature

Acronym	Definitions	Symbols	Definitions
ASTM	American Society for Testing and Material	l_{xa}	Pixel length without thermal bridges (m)
CAL	Calculating value based using Data sheet	L	height of the wall (m)
CED	Canny Based Edge Detection	k	Proportionality constant($w / (m^2 - K)$)

CEN	European Committee for Standardization	k_c	Thermal conductivity of the fluid ($W m^{-1} K^{-1}$)
CFD	Computational Fluid Mechanics	N	Number of zones
DCI	Dominant Color Isolation	N	Number of pixels in IR image
DCM	Dominant Color Masking	P_r	Prandtl number
FN	False Negatives	Q_{curk}	Heat loss in the k^{th} zone
FP	False Positives	$q_{density}$	Heat flow rate per unit area ($W m^{-2}$)
GHP	Guarded hot plate	$q_{o,s}$	Outgoing heat flow rate per unit area ($W m^{-2}$)
HFM	Heat Flux Meter	Q_{id}	Heat flow without thermal bridge ($W m^{-2}$)
HPT	Heating pulse thermography	q_{xTB}	Difference between heat flow rate with and without thermal bridge for pixel x (W / m^2)
IR	Infrared	q_x	Heat flow rate of pixel x with thermal bridge ($W m^{-2}$)
ISO	International Standard Organization		Heat flow rate of pixel x without thermal bridge ($W m^{-2}$)
LT	Local Thermography	Q_{tb}	Heat flow with thermal bridge ($W m^{-2}$)
MEAS	Measured using HFM	R	Thermal resistance ($(m^2 - K) / W$)
ND	North Dakota	R_{si}	Internal surface thermal resistance of the air boundary layers ($m^2 - K / W$)
NDT	Non-Destructive testing	R_{se}	External surface thermal resistance of the air boundary layers ($m^2 - K / W$)
NMMS	Non-maximal suppression	R_a	Rayleigh number
SML-HT	Sine Modulation lamp heating Thermography	S_k	k^{th} measuring area (m^2)
TAB	Using Analogies from coeval buildings	s_i	Material thickness
UAV	Unmanned aerial vehicles	s	Thickness of the material (m)
UND	University of North Dakota	T_s	Surface temperature (K)
Symbols	Definitions	T_p	Temperature of each pixel obtained from IR image (K)
A	Area of the entire wall (summation of all A_i 's) (m^2)	T_{sx}	Surface temperature at pixel x with bridges (K)
	Area of each pixel in IR image (m^2)	T_{sxa}	Surface temperature at pixel x without bridges (K)

	Heat transfer area (m^2)		Internal air temperature (K)
C	Specific Heat Constant		External air temperature (K)
d	Specimen thickness	T_{si}	Internal surface temperature (K)
d_k	Thickness (m)	T_{refl}	Reflected surface temperature of area (K)
F_j	View factor constant	T_m	Mean Temperature (K)
h_i	Internal Convective Coefficient		Thermal diffusivity (m ² =s)
h_e	External Convective Coefficient	U	Thermal transmittance coefficient $W / (m^2 - K)$
h_{si}	Internal surface heat transfer coefficient ($W / (m^2 K)$)	w	Water Content present in the element (%)
h_{ID}	Heat transfer coefficient	α_c	Convective heat loss coefficient
	External surface heat transfer coefficient ($W / (m^2 K)$)	α_r	Radiative Heat loss coefficient
	Convective with thermal bridges	ϵ	Emissivity
h_{cxa}	Convective without thermal bridges	γ	Dry density (g / cm ³)
h_{rx}	Radiative coefficient with thermal bridges	λ_k	Thermal conductivity for k th layer
h_{rxa}	Radiative coefficient without thermal bridges	ϕ	Heat flow(W)
h_i	Internal convective heat transfer coefficient	Ψ	Thermal bridge heat flow rate per unit temperature difference ($W / m - K$)
h_e	External heat transfer coefficient	ρ	Density (m^{-3})
h_{ce}	External convective heat transfer coefficient	σ	Stefan-Boltzmann constant
	Incidence factor of Thermal Bridge	τ	Duration of heat loss (s)
	Pixel length with thermal bridge(m)		

The qualitative assessment of buildings using thermal images captured by Infrared (IR) cameras mounted over Unmanned Aerial Vehicles (UAVs) has been successful in detecting moisture, cracks, insulation quality, and air leakage. In this technique, IR cameras are used to evaluate the overall thermal performance of the entire building (mostly outdoor environments). IR thermography-based approaches are gaining attention in the literature due to their ease-of-use, less cost, time, and efforts. Availability of

affordable IR cameras and the use of UAVs has the potential to revolutionize the process of thermal assessment for buildings.

In quantitative measurements, heat loss is typically quantified using indices such as the heat transmittance coefficient (U-value) or thermal resistance. The U-value is defined as the rate of heat flow across one sq. meter of a surface when there is a temperature difference of one Kelvin between the inside and outside surfaces. The U-value is measured in W/m^2K or BTU/ $^{\circ}F\ ft^2\ hr$. The thermal resistance or R-value is defined as the amount of resistance provided by the building element for a specific thickness to the overall heat flow. Section 3 details different quantitative indices (U, Q, R, λ, I) used for various building elements.

These assessment methods, however, are susceptible to external environmental conditions and measurement errors may occur due to factors such as: (1) surface properties like emissivity, roughness, reflexivity, stains, and colors; (2) environmental factors such as incident solar irradiance, cloud presence, humidity, ambient temperature, moisture, and wind speed; and (3) miscellaneous factors that include distance, field of view, building orientation, and presence of unwanted objects (e.g. trees, ground, and sky) [4–9]. Measurement errors, however, can be minimized by adopting recommendations from standards such as ISO Directive 2012/27/UE [10, 11], CEN [E-1213] [12], and ASTM (E-1543) [13–17]. Their recommendations include (1) positioning of camera perpendicular to the building; (2) wind speed must be less than 5 m/s [18, 19]; (3) temperature difference between the internal and external wall surface should be at least $10^{\circ}C$; and (4) the inspected surface must ideally be free from any solar radiation. Thus, aerial inspections using UAVs equipped with an IR camera can be considered as a suitable approach to perform thermal assessments of buildings.

Figure 1. Classification of thermal performance assessment of buildings

There are limited existing comprehensive surveys available for the qualitative and quantitative heat-loss estimation techniques. Our extensive state-of-the-art literature review show that the availability of affordable light-weight IR cameras and UAVs can revolutionize the process of thermal assessment for buildings. Thermal assessment for small and medium-sized buildings using IR-based aerial thermography is a relatively straightforward process compared to high-rise buildings [20]. Moreover, IR-mounted UAVs consume less time and cost and can be stretched to hard-to-reach areas (e.g., roofs and underground structures). For this paper, we analyze medium-sized buildings with building area ranging from 30,000 to 50,000 sq. ft.

This paper contributes to the following specific aims:

- A comprehensive review and classification of thermal measurement techniques based on type, method, application, and quantification indices.
- A novel data-driven, three-layered (database, pre-processing and automation, and evaluation) framework for estimation of heat-loss using UAS-based thermal imagery.
- Machine learning based techniques (Mask R-CNN) to detect and segment building elements and to accurately quantify the heat-loss (or U-value) by processing thermal images (~ 5000 thermal images were captured on the UND campus).

The remainder of the paper is organized as follows: Section 2 provides a broader classification of qualitative or quantitative thermal performance measurement techniques and their applications with an exhaustive literature review; Section 3 classifies these measurement techniques based on the various quantification indices used for heat-loss estimation; Section 4 introduces a three-layered data-driven framework for UAS-assisted thermal-imagery based heat loss quantification; Section 5 discusses results for the proposed machine learning model and heat-loss evaluation; and Sections 6, 7, and 8 end with a conclusion, pointers for future work, and acknowledgment respectively.

2. Classification of Thermal Performance Measurement Techniques based on Measurement Type, Method, and Applications

This section reviews several measurement techniques that are currently available to assess thermal performance of building envelopes with specific emphasis placed on the measurement type, methods, and applications as shown in Fig. 1. Some of the case studies on assessment of overall thermal performance of buildings, detection of thermal bridges, moisture, and air leakage are discussed in detail (Table 2). The objective of this section is to provide a literature survey and discover the appropriate technique (over various parameters such as ease of deployment, cost effectiveness, time consumed, detection capability, environmental effects, and attainability) that exists in the literature to analyze the thermal performance of campus buildings.

2.1. Measurement Type

The thermal performance assessment techniques can be either passive or active type. Passive measurements are carried out by using data sheets or using similar buildings. On the other hand, in active measurement, variables like wall surface temperature, inside or outside air surface temperature, wind velocity, etc. are measured.

2.1.1. Passive Measurements

Passive measurements can further be divided into coeval buildings, theoretical approaches, and finite element analysis. In coeval buildings, thermal assessment is done for structures of similar age, geographical location, and material compositions [21–24]. This technique is applicable when the actual building measurement is not possible. However, this method is often challenging due to missing building information such as construction periods, material compositions, and wall thickness and texture [25–30]. In theoretical methods [31–33], the R-value (or U-value) of buildings is calculated from the thermal conductivity and thickness of individual layers of a wall [34]. Simulation based design for 3D building envelopes is considered in finite element analysis method [35, 36].

2.1.2. Active Measurements

Active measurement techniques can be classified into HFM based measurement, laboratory testing, and IR thermal imaging.

Table 2. Summary of qualitative measurements

Measurement Scope	Details of Data	Sensors	Methodology	Comments	Reference
	Collection and Accessories				
Outdoor qualitative measurements					
Building structure surveillance using an IR camera for possible degradation	IR camera was used to capture thermal images of outdoor building structures	IR camera	Non-destructive testing (NDT) method used for assessment of physio-chemical treatments such as stone cleaning, consolidation in historical	- No validation or sensitivity analysis	2002 [37], 2003 [38]

			structures and buildings		
Detection of moisture in various buildings using an IR camera	IR camera was used to capture thermal images for a duration of 600 hours Thermocouples were used to validate the results	IR camera, thermometer, thermocouples	Moisture detection was carried out using an IR camera thermometer and thermocouples under different conditions while varying time, distance and view angle	+ Validation shows 2.5-8.5% deviation from actual measurements + Sensitivity analysis for moisture detection was also carriedout	2016 [39] 2013 [40]
Detection of building thermal bridge using an IR camera	122 residential buildings in South West England were inspected for a duration of one month using IR cameras	IR camera	Pass by thermography: where an IR camera is mounted on top of a car to capture pass-by thermal images of building faces	+ Pass-by thermography is less expensive compared to walk-by thermography - No validation	2004 [41] 2016 [42]
Detection of air leakage for various buildings using IR cameras	IR camera was used to capture thermal images for a duration of 2 months	IR camera, temperature & humidity sensor, weather station	IR camera is used to detect air leakage through the roller shutter handle and the window frame of a room Portable fans were used to generate temporary pressure difference	+ Sensitivity analysis for varying pressure difference was carried out - No validation	2017 [43] 2013 [44]
Indoor qualitative measurements					
Assessment of thermal performance using an IR camera	Thermal images were captured using an IR camera	IR camera	NDT method was used for thermal performance assessment	+ Emissivity correction was carried out - Verification of the measurements was not provided	2016[45]
Detection of hidden cracks using an IR camera in a laboratory	EasyHeat 224 Ambrell induction heater system used for coil excitation.	IR camera, heater	Eddy current pulsed thermography: heat is generated using heater	- No validation	2016 [46]

environment	SAT-HY6850 thermal camera used to record the thermal responses of the specimen for the duration of 2.4 secs		system and thermal camera captures the anomaly to detect the hidden cracks		
-------------	---	--	--	--	--

Figure 2. Infrared thermal imagery: (a) aerial inspection using an Airbus plane [47]; (b) aerial inspection using an Airbus helicopter [48]; (c) automated fly inspection using UAVs [49]; (d) street drive inspection using vehicle [50]; (e) hand-held IR camera used for general walk through inspection [51]

2.1.2.1. HFM Measurements

In this test, heat flow of the inspected element is measured using a Heat-Flux Meter (HFM) which consists of thermistors, transducers, a heat-flux plate (or heat flux sensor), and a data-logger [52–59]. The measurement accuracy depends on the type of instruments, installation procedure, data-capturing, and calibration mechanisms which includes position of the measurement apparatus, non-homogeneity of the materials, and the amount of water or moisture present in the material [60–66]. It is highlighted that solar radiation can interfere with HFM measurements. Hence, the measurements were carried out during dawn or dusk [64–66]. If the heat flow between the interior and exterior is low or the temperature difference is lower than 10 °C, then measurements taken may not be accurate [64–66].

Laboratory Testing. In laboratory testing, the thermal performance of a wall specimen is evaluated in a controlled lab environment [67–70]. In this environment, HFM or guarded hot plate (GHP) based lab equipment is used to measure the thermal performance according to the International Standard ISO 8301 [64–66]. The measured heat flow rate from GHP combined with temperature difference are used to estimate the U-value [69, 71, 71–80].

IR thermal imaging. In IR thermal imaging, the thermal performance of a grey body is typically quantified using indices such as the U-value, R-value, etc. [10–17, 81, 82]. These indices can evaluate structural properties such as thermal bridges, emissivity of building facades, roofs, windows, and glazing systems.

The advantages of using an IR camera include nondestructive measurement, coverage of a larger inspection area in limited time, immediate access to raw surface temperature data, and acquisition of continuous imagery that can be logged remotely. However, environmental factors such as humidity, wind speed, air temperature, and solar radiation can limit the accuracy in estimating the surface temperature [83].

2.2. Qualitative and Quantitative Methods

The measurement techniques can be divided into qualitative or quantitative. Qualitative measurements are helpful in evaluating the overall thermal performance of buildings by identifying locations of maximum heat loss and/or possible thermal bridges, or assessing the quality of the thermal insulation, without quantifying the thermal loss [84, 85]. A summary of various indoor and outdoor qualitative measurements are given in Table 2. Table 2 denotes the details of data-collection, measurement type, and methodology. The “Comments” column shows positive (+) and negative (-) aspects for each method. These methods are effective due to their lesser processing times, costs and efforts [86]. Uneven thermal patterns created by moisture or dampness can also be detected using qualitative measurements. The water content hidden in the wall acts as storage of additional heat and affects the overall thermal performance. The effect of air leakage can also be detected using qualitative thermal measurements.

The most cited heat loss coefficient in literature is the U-value, and it is defined as the rate of heat flow across one square meter of a surface when there is a temperature difference of one Kelvin [87] between the inside and outside surfaces (or vice-versa) and is expressed in W/m^2K . Hence, we adopted U-value as the quantitative metric to estimate the heat-loss for our UAV based building data sets (e.g., Twamley and Museum).

Based on the type of apparatus used, the qualitative and quantitative assessment techniques can be further categorized into global IRT, non-IRT, and heating source based evaluation.

2.2.1. Global IRT

In this technique, IR thermography is used to evaluate the overall thermal performance of the entire building (mostly outdoor environments). Hence, these techniques are susceptible to the external environmental conditions. These techniques can be divided into aerial inspection, unmanned aerial vehicle inspection, street drive inspection, and walk through inspection (see Fig. 2).

Aerial inspections [88, 40] (see Fig. 2) refer to the use of IR cameras installed on an airplane or a helicopter. Automated fly inspection measurements use an IR camera mounted on an (automated) UAV (see Fig. 2) without human interventions. These techniques suffer from licensing restrictions, higher equipment costs and drone vibrations [88]. Thermal images are captured using an IR camera mounted on a vehicle which runs through various streets or roads in street drive inspection [88, 42, 89]. MIT (Massachusetts Institute of Technology) developed a system called the “kinetic super resolution process” that can capture high resolution thermal images using a slow driving vehicle which is more cost effective than walk through inspection [42, 90]. In walk through inspection (see Fig. 2), a thorough scan of different faces has been carried out by walking around the building with a hand-held IR camera [86]. This technique is also applicable for internal thermal performance assessment, however it consumes more time and effort. In addition, the thermal videos can capture possible temporal effects [91–93]. In general, the IRT techniques require uninterrupted power and can be impacted by the presence of obstacles. Moreover, the external approaches are susceptible to environmental conditions [85].

However, in these methods, measurement errors may occur due to different reasons such as: (1) surface properties like emissivity, roughness, reflexivity, stains, and colors; (2) environmental factors such as incident solar irradiance, cloud presence, humidity, ambient temperature, moisture, and wind speed; and (3) miscellaneous factors that include distance, field of view, building orientation, and presence of unwanted objects (e.g. trees, ground, and sky) [4–9].

Figure 3. Comparative figure showing (a) different thermal patterns caused by moisture during day, and (b) during night [39]; (c) weak/strong insulation of building wall [94]; (d) component anomalies: frame within wall is visible [95, 96]; (e) structural anomalies detected near windows, junctions between two external walls, and pillar joints [97]; and (f) air leakage detected from thermal images [44]

The measurement errors, however, can be minimized by adopting standards such as ISO Directive 2012/27/UE [10, 11], CEN [E-1213] [12], and ASTM (E-1543) [13–17]. Their recommendations include (1) positioning of camera perpendicular to the building; (2) wind speed must be less than 5 m/s [18, 19]; (3) temperature difference between the internal and external wall surface should be at least 10 °C; and (4) the inspected surface must ideally be free from any solar radiation. Thus, aerial inspections using UAVs equipped with an IR camera can be considered as a viable option for thermal assessments of buildings.

2.2.2. Non-IRT

The non-IRT based methods can be divided into HFM based techniques and laboratory testing whereas in laboratory measurements, the thermal performance of a wall specimen is evaluated in a controlled lab environment using HFM or Guarded Hot Plate (GHP) based lab equipment [67–70].

n								
Window/Door Inspection	No	No	No	Yes (limited)	Yes	Yes (limited)	Yes (limited)	Yes
Type	QN	QN & QL	QN	QN & QL	QN & QL	QN & QL	QN & QL	QN & QL
References	[52–59]	[46, 98]	[67–70]	[7]	[88, 40]	[6, 7]	[91–93]	[42, 90]

Table 3. Characteristic review of qualitative and quantitative IRT and non-IRT techniques

2.2.3. Heating Source

Sometimes, heating sources are used in combination with IRT or non-IRT measurements. One or more heating sources is used to heat the surface of a test specimen in order to capture the thermal anomaly in the transient phase. The thermal anomalies, like hidden cracks or moisture, can be captured using an IR camera or an HFM in the presence of a heater. Based on the type of heating source, these techniques can be categorized as Heating Pulse Thermography (HPT), Sine Modulated Lamp Heating Thermography (SML-HT), and laser thermography.

In HPT, a pulse of short duration from a heater is applied on the inspected object. The temperature variation during transient states of heating and cooling is recorded using an IR camera [99]. An alternative heating source based on eddy current is used in [46]. In SML-HT, heat is applied periodically using a sine modulated lamp to produce the temperature variations [4, 5]. In laser thermography, the laser beams are used as a heating source [6, 7].

2.3. Applications

Based on the applications, different thermal measurement techniques can be used for overall building evaluation, thermal bridge assessment, moisture detection, assessment of insulation, and assessment of air leakage (Fig. 3).

2.3.1. Assessment of Overall Thermal Performance

The thermal performance evaluation helps in assessing the overall thermal conductivity (ability of a specific material to conduct heat), heat capacity, thermal emissivity (effectiveness in emitting energy as thermal radiation), thermal diffusivity (temperature spread through the surface), and material density of buildings [86]. These measurements can be carried out for shorter or longer duration.

The short term measurements need to comply with the international standards developed by International Standard Organization (ISO) [10, 11], European Committee for Standardization (CEN) [12], and American Society for Testing and Material (ASTM) [13–17]). Short time measurements are generally conducted from few hours to several months and are useful in evaluating various properties of the wall, like age [100, 38], constituent materials [101, 37, 30], thickness [84, 102], geometry [44, 30, 45], surface properties of the wall [30], and sub-components and their alignment within the wall [86].

The long term measurements are valuable in providing deeper insights into the progression of the thermal anomalies, and these measurements typically continue for several years [103–105]. The building degeneration assessment due to the presence of moisture over a period of several years is an example of a long-term measurement technique [106, 107].

2.3.2. Detection of Thermal Bridges

Thermal bridges are defined as an area having a higher thermal conductivity than the surrounding areas, thereby providing less resistance to heat transfer. The two types of thermal bridges are structural and component. The structural bridge is formed by the building structures such as junctions and connections between two external walls, roof or floor joints, window joints, pillar joints, etc. (see Fig. 3). The component bridge, as shown in Fig. 3, is created by the abnormalities present in the materials or the problems associated with alignment of various components such as timber stud, steel wall ties, etc. [18, 34, 44, 108–112].

2.3.3. Detection of Moisture and Water Content

Moisture, dampness or water content on walls can result in evaporative cooling and can create uneven thermal patterns which can be detected by an IR camera [39, 34]. The moisture or dampness detection can help in corrective measures for increasing the lifetime of buildings and removing the chances of any biological bacterial growth.

The best time to detect any possible water trace in the outside wall is in the early evening after a sunny day. As the solar radiation aids the evaporation process, the water traces can be easily captured using IR cameras [34] (see Fig. 3). In [113], laboratory experiments are carried out for moisture detection using additional cooling and heating system. Thermal performance assessment techniques can identify the water traces. However, these methods have limitations with respect to specific environmental conditions. Additional tools such as moisture meter and calcium carbide sampling can be used to increase the detection accuracy [39, 113].

2.3.4. Assessment of Thermal Insulation

Qualitative and quantitative measurements are effective for the assessment of an insulation system. Specifically, these measurements can be used to detect absence of the insulation materials [34, 85, 41, 114], non-working or damaged insulation components [114, 84, 34, 115], and misaligned insulation components [34] (see Fig. 3). Damage of the insulation is caused by the detachment, shrinkage, low adhesion [44], and cracking of board panels, and finishing systems abnormalities [116]. In order to capture these defects, the standard procedures include maintaining a temperature difference of at least 10 °C between the internal and external wall for at least four hours before assessment [116].

2.3.5. Detection of Air Leakage

Air leakage affecting the overall temperature gradient of the wall surface can be captured using IR cameras (see Fig. 3) [44, 117, 118]. The impact of air leakage on the temperature gradient increases with the magnitude and size of the leakage [34, 43]. The air leakage can be detected successfully if the temperature and pressure difference between inside and outside building (or wall) is at least 10 °C and 10 Pascals, respectively [43, 44]. Generally, a mechanical device like a fan or ventilation system is used to create an artificial pressure difference [119, 120].

A detailed comparison of various quantitative approaches used for indoor and outdoor measurements is given in Tables 4 and 5 respectively. These tables provide a summary of the scope of measurement, data collection process, errors, sensor type, quantification indices, advantages and limitations, and relevant references in the literature review. In these studies, different measurement apparatus such as IR cameras, HFM, thermometers, thermocouples, and weather stations were used to estimate the temperature distribution, total heat loss, thermal transmittance, conductivity, and amount of thermal resistance of the building. In addition, actual measurements are carried out to aid in the credibility of these techniques.

The qualitative and quantitative heat-loss estimation techniques are compared in Table 3. The heat-flux meter based techniques are suitable for laboratory setup, but require additional instruments. Hence, these techniques requires more cost and time if deployed to conduct building heat loss survey. The HFM based techniques are effective for surface anomaly detection. The advantages of using such techniques are that they produce more accurate results and are not susceptible to environmental (or vibration) effects.

Moreover, these techniques are applicable for quantitative surveys as they can estimate the heat-flux (Q) using HFM. Similarly, the guarded hot-plate (GHP) based techniques can estimate the heat-flux accurately at a cost of increasing time and efforts. The GHP based estimation uses a guarded heater and air-flow to measure the heat-flux in a controlled lab environment.

The Heating Pulsed Thermography (HPT) based techniques require additional instruments (such as heaters) to identify hidden anomalies (such as cracks) using an IR camera. The presence of an IR camera, heater and other instruments makes it difficult to conduct a building heat-loss survey. The HPT techniques can heat-up the inspected elements more quickly than HFM or GHP based techniques. The Lock-in Thermography (LT) based techniques apply a sine-modulated lamp heating over the inspected elements to produce a temperature difference. These methods are effective to identify hidden anomalies, and can be used to estimate the heat-loss of buildings, but requires additional setup. Laser spot thermography techniques use laser beams to generate external heat and can identify surface cracks. These techniques (HPT, LT, LST) can be applied to both qualitative and quantitative surveys.

The aerial or UAV/assisted IRT techniques are cost-effective and consume less time for set-up. These techniques help detect any presence of surface anomalies (e.g., cracks, leaks, or moisture levels) without the need for any external heating source. These techniques are also useful in conducting building surveys (including the roof). The street-drive IRT techniques are cheap compared to UAV-assisted IRT techniques, but trying to conduct full building surveys (especially the roof). Walk-through IRT techniques consume more time but are highly flexible. However, the UAV-assisted IRT techniques are easy to deploy, cost-effective, less time consuming, non-destructive, and can be extended for hard-to-reach areas. Hence, in this work, we utilize the UAV-assisted IRT technique for heat-loss assessment of the various campus buildings.

Table 4. Summary of quantitative outdoor measurements

Auth or	Ye ar	Buil ding elem ent anal yzed	Equipm ent used for measurement	Measur ement duratio n	Valida tion	% Err or	T_{refl} compensation	ϵ -measur ement	Sensit ivity analys is	Comment s
Quantification Index - Heat Transfer Coefficient (U)										
Alba tici et al. [63]	20 08	Wall surfa ce	IR camera, anemom eter, heater	NA	CAL	32	NA	Y	NA	- No sensitivi ty analysis
Alba tici et al. [121]	20 10	Wall surfa ce	IR camera, soldering iron, anemom eter	NA	CAL MEAS	30- 161 53	NA	Y	NA	+ Accurat e results obtained by avoiding solar radiatio n, with

										10K temperat ure differen ce
										& minimu m wind velocity
Tayl or et al. [44]	20 13	Build ing	HFM, thermom eter	7-14 days	CAL	2- 154	NA	NA	NA	+ On- site assessm ent during building construc tion for preventi ve analysis
Dall et al. [122]	20 13	Build ing	IR camera	NA	CAL	2- 154	Y	Y	NA	+ Used for energy audit application
Nard i et al. [123]	20 14	Build ing	IR camera, hosespip e	24 days	CAL MEAS	29 38	NA	NA	NA	+ IRT results are verified using theoretic al and HFM measure ments - No sensitivi ty analysis
Nard i et al [124]	20 15	Wall surfa ce	IR camera, hosepipe	NA	CAL MEAS	46 47	Y	Y	NA	+ Differen t thermal

										mass of walls considered
										- No sensitivity analysis
Albatici et al. [125]	2015	Wall surface	IR camera, weather station, thermo-hygrometer	1 hour	CAL MEAS	23 22	NA	NA	Y	+ IRT results were validated using HFM measurement - Sensitivity analysis showed IRT estimation deviates by 9%, 27%, and 50% when the wind, inner and outer temperature deviate by 9% respectively
Choi et al.	2017	Wall surface	IR camera, anemom	NA	CAL ME	1-4	Y	Y	Y	+ Sensitivity

			eter		AS	4 5- 4 2					analysis, + Reflected temperature compensated
Quantification Index - Thermal Resistance (R)											
Mad ding et al. [126]	20 08	Wall surfa ce	IR camera, weather station	24 hours	MEAS	12	Y	NA	Y	+ Temper ature differen ce is highligh ted as most influential	
Ham et al. [127]	20 14	Build ing	IR camera, optical camera, thermometer	NA	NA	NA	NA	NA	NA	+ Building 3D model was constructed using thermal and digital imagery	
Ibos et al. [128]	20 15	Wall surfa ce	IR camera, weather station, thermocouples, emissometer	3-7 days	CAL MEAS	57 60	NA	Y	NA	+ Emissiv ity measure d using emissometer - No sensitivi ty analysis	

Mari no et al. [87]	20 17	Build ing	IR camera, laser distance meter, thermome ter, thermo- resistanc es, weather station	4 days	NA	NA	Y	Y	NA	+ Evolutio n of spatial thermal resistanc e was shown
Quantification Index - Total heat loss (Q)										
Ghia us et al. [129]	20 06	Build ing	NA (using weather data and building energy consump tion model)	1 month	NA	NA	NA	NA	NA	+ Regressi on based model from weather data
Vavi lov et al. [115]	20 10	Wall surfa ce	IR camera, heat gauge sensor, temperat ure sensor	236 days	CAL MEAS	3- 193 10	NA	NA	NA	+ Validat ed using HFM measure ment
Voll aro et al. [130]	20 15	Build ing	IR camera (and building data sheet)	8640 hours	MEAS	12- 14	NA	NA	NA	+ Results obtained from data sheet are validat ed using HFM measure ments and an IR

											camera
Quantification Index - Temperature distribution coefficient (T_d)											
Kim et al. [131]	2016	Building	IR camera	12 months	NA	NA	NA	NA	NA	- No validation or sensitivity analysis performed	

Table 5. Summary of quantitative indoor measurements (part I)

Author	Year	Building	Equipment used	Measurement	Validation	% Error	T_{refl} compensation	ϵ -measurement	Sensitivity	Comments
				for measurement	duration					
				analyzed						
Quantification Index - Heat Transfer Coefficient (U)										
Kato et al. [132]	2007	Wall surface specimen	IR camera	5 days	MEAS	6	NA	NA	NA	+ Validated using HFM measurements - No sensitivity analysis
Grinzato et al. [133]	2010	Wall surface	IR camera, anemometer	NA	CAL MEAS	8-114 8-95	NA	NA	NA	- No sensitivity analysis - No emissivity correction
Fokaides	20	Wal 1	IR	3 hours	CA	5	NA	NA	Y	+ Validate

et al. [33]	1 1	surf ace spec ime n	camera, thermoh ygrometer		L ME AS	9 2 1				d using thermoh ygrometer and HFM
										+ No sensitivi ty analysis
Tho uven el et al. [134]	2 0 1 2	Wall surfac e	IR camera, thermoc ouple	10 hours	CAL	5	NA	Y	NA	+ Emissivi ty correcti on
										provide d
										- No sensitivi ty analysis
Ham et al. [135]	2 0 1 3	Wall surfac e	IR camera	NA	NA	NA	NA	NA	NA	-No emissivi ty correcti on
										-No sensitivi ty analysis
Ohls son et al. [136]	2 0 1 4	Wall surfac e	IR camera, hosepipe, anemomet er	1 hour	MEA S	NA	NA	NA	NA	+Validat ed using HFM
										measure ment
										- No emissivi ty correcti on
										- No sensitivi ty analysis
Sim	2	Wal	IR	1 hour	MEA	36	NA	NA	Y	+ HFM

oes et al. [137]	0 1 4	1 surf ace spec ime n	camera, thermoc ouples, anemom eter	S						measure ments used to validate results + Sensitivi ty analysis showed the effect of emissivi ty
Tzif a et al. [138]	2 0 1 4	Wall surfac e speci men	IR camera, thermomet er	24 hours	CAL	2- 204	Y	Y	NA	+ Emissivi ty correcti on was made using vinyl black tape, + Reflecte d temperat ure was consider ed + Validate d using CAL method + Uncertai nty quantifi cation using U- value assessm

										ent
Nardi et al. [123]	2014	Wall surface specimen	IR camera	2 days	NA	NA	NA	NA	NA	- No sensitivity analysis
Nardi et al. [124]	2015	NA	IR camera, hosepipe, thermos-hygrometer	NA	CAL MEAS	7 13	NA	NA	NA	+ IRT measurements validated using HFM measurements - sensitivity analysis missing
Nardi et al. [139]	2016	Wall surface	IR camera, thermo-hygrometer, hosepipe	1 hour	CAL MEAS	3 9 2 0	Y	Y	Y	+ Four different equations were compared + Sensitivity analysis and emissivity correction carried out
Donatelli et al. [98]	2016	Wall surface	IR camera, thermo-hygrometer, halogen lamps	10 hours	CAL	4	Y	Y	NA	+ Pulsed heating technique with halogen lamps

				anemometer								was used
												+ Emissivity correction
												- No sensitivity analysis
Tejedor et al. [140]	2017	Wall surface	IR Camera, thermometer, hygrometer, thermocouple	2-3 hours	TA B CA L ME AS	4 2 - 20 1 2 - 27	Y	Y	Y		+ Emissivity correction and sensitivity analysis were carried out	
Marshall et al. [141]	2018	Wall surface	IR camera	NA	TA B ME AS	2 - 27 9	Y	Y	NA		+ Emissivity correction was carried out + IR images with different resolution were captured	

Table 6. Summary of quantitative indoor measurements (part II)

Auth	Y	Buil	Equip	Measu	Valid	%		ϵ -	Sensi	Commen
------	---	------	-------	-------	-------	---	--	--------------	-------	--------

or	ea r	ding	ment used	remen t	ation	Error	T_{refl}	measu remen t	tivity	ts
Quantification Index - Thermal Resistance (R)										
Kisil ewik z et al. [142]	20 10	Wall surface	IR camera, reflector, thermoco uples	48 hours	MEA S	43	Y	NA	NA	+ Emiss ivity measu rement were carried out - Sensiti vity analysi s missin g
Nardi et al. [143]	20 14	Wall surface	IR camera	NA	MOD	73	NA	NA	NA	- Sensiti vity analysi s and emiss ivity correct ion were missin g
Ibos et al. [128]	20 15	Wall surface	IR camera, weather station, thermoco uples, emissom eter	3-7 days	CAL MEA S	57 60	NA	Y	NA	+ Emiss ivity measu red using emiss ometer

										- Sensitivity analysis missing,
Donatelli et al. [98]	2016	Wall surface specimen	IR-camera, thermo-hygrometer, halogen lamps, anemometer	13 hours	CAL	4	NA	NA	Y	+ IR camera measurement were validated using HFM measurements + Sensitivity analysis was carried out

Quantification Index - Total heat loss (Q)

Danielski et al. [83]	2015	Wall surface specimen	IR-camera, thermometer	143 days	MEAS	11	NA	NA	NA	+ IRT measurements were validated using HFM measurements
-----------------------	------	-----------------------	------------------------	----------	------	----	----	----	----	---

Quantification Index - Thermal Bridge ()

Asdrubali	2012	Doors, Windo	IR-camera	NA	MEAS	5	NA	Y	NA	- No sensitivity
-----------	------	--------------	-----------	----	------	---	----	---	----	------------------

et al. [61]		ws	, thermo meter						+ Emissi vity calibra tion	
O'gr ady et al. [144]	20 17	Wall surface	IR- camera, anemome ter	NA	MEA S	36	Y	Y	Y	+ Sensiti vity analysi s
O'gr ady et al.[1 45]	20 17	Wall surface	IR- camera, anemome ter	NA	MEA S	12	NA	NA	NA	+ Valida ted using HFM
										+ Emissi vity correct ion
										- Sensiti vity analysi s, correc tion were missin g

										Validated using HFM
Baldinelli et al. [146]	2018	Wall surface	IR camera, temperature probes	NA	MEAS	52	Y	Y	NA	+ Emissivity correction carried out - Sensitivity analysis was missing

Quantification Index - Thermal Conductivity (λ)

Wan g et al. [73]	20 18	Wall surface	HFM, heatin g circuit s, thermo couple	72 hours	CA L	2 - 2 7	NA	NA	NA	+ Resul ts we re verifi ed usin g theoret ical metho ds
					ME AS	9				- Sensiti vity analysi s missin g

3. Heat-flow Calculations, Thermal Conductivity, and Resistance, and Transmittance Indices

This section details the process of heat-flow calculations focusing on thermal conductivity, temperature distribution, total heat loss, incidence factor of the thermal bridge, thermal resistance, and the thermal transmittance coefficient. The objective of this section is to investigate existing techniques for heat-loss quantification and emerge the best suitable quantification index for assessment of the campus buildings later in section 5.

3.1. Thermal Conductivity

This index can be used to identify thermal anomalies like cracks, moisture, etc. The thermal conductivity (λ) can be measured using the thermal diffusivity (d_t) as given in the following equation [147]:

$$\lambda = \rho C d_t \quad (1)$$

where ρ and C denote the mass density and the specific heat constant, respectively. The thermal conductivity can be evaluated from the amount of heat flow [73] as given by

$$\lambda = \frac{\Phi d}{(T_{si} - T_{se}) A} \quad (2)$$

where ϕ and d are the heat flow and specimen thickness, respectively, and are measured using laboratory equipment.

3.2. Temperature Distribution Coefficient

Hidden cracks can be identified using the temperature distribution coefficient. This method is applicable for homogeneous and isotropic materials. The spatial temperature distribution across the surface element for a 2D homogeneous surface must satisfy the following equality:

$$\frac{\partial^2 T}{\partial x^2} + \frac{\partial^2 T}{\partial y^2} = \frac{1}{d_t} \frac{\partial T}{\partial t} \quad (3)$$

where $T=T(x,y,t)$ denotes the surface temperature in x, y coordinates, and t denotes the time domain. The diffusivity constant can be given from Eq. 1. The cracks can be identified from those vicinity where Eq. 3 is not satisfied. The temperature difference can also be used for cracks and air leakage estimation [148, 149].

3.3. Total Heat Flow Measurements

The total heat loss, or heat flow, (Q) in a building element can be quantified using the following equation [115]:

$$Q = \sum_{k=1}^N Q_{cur,k} \tau S_k \frac{T_{air}^{in} - T_{air}^{out}}{T_s^{in} - T_{air}^{in}} \quad (4)$$

Figure 4. The process of dividing the building into K zones [115]

where $Q_{cur,k}$ is the heat loss in the k^{th} zone (measured using a heat gauge sensor, see Fig. 4), τ is the duration of heat loss, N is the number of zones, and S_k is the k^{th} measuring area. An IR camera is used to capture the surface temperature T_s^{in} and the air temperature is measured using a thermometer. This method combines IR camera and heat gauge sensor technology. In [83], the Q -value is quantified as:

$$Q = \epsilon \sigma (T_{hot}^4 - T_{cold}^4) + \alpha_c (T_{hot} - T_{cold}) \quad (5)$$

where T_{hot} and T_{cold} denote the temperature of hot and cold sides of the wall, respectively. The density of heat flow rate (which is heat flow rate per unit area, Wm^{-2}) is used as the quantification index in [136] and it is given by

$$q_{density} = q_r + q_c \quad (6)$$

where $q_r = q_{o,s} - q_{i,s}$, $q_{o,s}$ and $q_{i,s}$ denote the outgoing heat flow rate and incoming heat flow rate (per unit area), respectively, and they are expressed as

$$q_{o,s} = \epsilon \sigma T_s^4 + (1 - \epsilon) q_{i,s} \quad (7)$$

$$q_{i,s} = \sum_j F_j q_{o,s,j} \quad (8)$$

where F_j is a constant and $q_{o,s,j}$ is the outgoing heat flow rate per unit area for the surface j .

3.4. Incidence Factor of Thermal Bridge (I_{tb})

This index evaluates the performance of a building element by comparing it with an ideally insulated building material. It is used to quantify the performance of a thermal bridge and can be given as the ratio of heat flow with and without thermal bridges [61]

$$I_{tb} = \frac{Q_{tb}}{Q_{ID}} \quad (9)$$

where Q_{tb} and Q_{ID} denote the heat flow with and without thermal bridge, respectively, and can be expressed as

$$Q_{ID} = h_{ID} A_{ID} (T_{ai} - T_{si}) \quad (10)$$

where h_{ID} and A_{ID} are the heat transfer coefficient and heat transfer area, respectively, and

$$Q_{tb} = h_{tb-i} A_p \sum_{p=1}^N T_i - T_p \quad (11)$$

where h_{ID} , A_p , N , and T_p represent the heat transfer coefficient with thermal bridge, area of each pixel, number of pixels, and temperature of each pixel obtained from IR images, respectively. In [146], the incidence factor of thermal bridge, I_{tb} , is estimated as

$$I_{tb} = \frac{\sum_{x=1}^N (T_{ai} - T_{sx})}{N (T_{ai} - T_{sxa})} \quad (12)$$

where N is the number of pixels.

In order to assess the overall performance of a thermal bridge, O'Grady et al. [144, 145] investigated the thermal bridge heat flow rate per unit temperature difference (Ψ) which is expressed as

$$\Psi = \frac{q_{TB}}{T_{ai} - T_{ae}} \quad (13)$$

where q_{TB} denotes the thermal bridge heat flow rate, given by

$$q_{TB} = \sum_{\forall x} q_{xTB} \quad (14)$$

where q_{xTB} represents the thermal bridge heat flow rate for pixel x and it can be estimated as the difference between the heat flow rate of pixel x with (q_x) and without (q_{xa}) thermal bridges using the following expression:

$$q_{xTB} = q_x - q_{xa} \quad (15)$$

Here, q_x and q_{xa} can be expressed as,

$$q_x = l_x [(h_{cx} + h_{rx}) | T_{ae} - T_{sx} |] \quad (16)$$

$$q_{xa} = l_{xa} [(h_{cxa} + h_{rxa}) | T_{ae} - T_{sxa} |] \quad (17)$$

where $l_x, l_{xa}, h_{cx}, h_{cxa}, h_{rx}, h_{rxa}, T_{sx}$ and T_{sxa} are pixel length with and without thermal bridges, convective and radiative coefficient with and without thermal bridges, and surface temperature at pixel x with and without bridges, respectively.

3.5. Thermal Resistance

The thermal resistance or R-value is defined as the amount of resistance provided by the building element for a specific thickness to the overall heat flow. Therefore, when the R-value increases, the building element provides better insulation. The R-value is expressed in $m^2 - K / W$. This section provides details of various indices used to quantify the thermal resistance. The R-value can be estimated as the ratio of material thickness (s_i) to conductivity [150] (λ_i) as shown by

$$R = \frac{s_i}{\lambda_i} \quad (18)$$

Equation 18 shows the resistance for material i . If thermal conductivity and material thickness are not available, the resistivity can be estimated by

$$R = \frac{T_{ae} - T_{ai}}{4\epsilon\sigma T_m^3 (T_{si} - T_{refl}) + \alpha_c (T_{si} - T_{ai})} \quad (19)$$

[126, 135]. The following equation is used to quantify the resistivity coefficient in [98],

$$R = \frac{T_{ai} - T_{ao}}{5.67\epsilon \left[\left(\frac{T_{wc}}{100} \right)^4 - \left(\frac{T_{out}}{100} \right)^4 \right] + \alpha_c (T_{wc} - T_{out})} \quad (20)$$

In multi-layer buildings, the resistivity can also be quantified as the summation of resistances in different layers as shown by

$$R = R_{si} + \frac{e}{k} + R_{se} \quad (21)$$

where R_{si} , R_{se} , s , and k denote the internal and external surface thermal resistances of the air boundary layers, thickness of the material, and proportionality constant (defined as the amount of heat that flows through a unit thickness of the material, $\frac{W}{m^2 K}$, and can be retrieved from the material properties), respectively. In [65], the internal and external surface thermal resistances are replaced by the internal and external convective heat transfer coefficients, h_i, h_e , respectively, as follows:

$$R = \frac{1}{h_i} + \frac{e}{k} + \frac{1}{h_e} \quad (22)$$

3.6. Thermal Transmittance Coefficient

The thermal transmittance coefficient or the U-value of an internal wall surface is quantified in [132] as the ratio of total heat flow to the temperature difference:

$$U = \frac{\sum_{\forall i} \alpha_c (T_{ai} - T_{si}) + \alpha_r (T_{refl} - T_{si}) \times A_i}{(T_{ai} - T_{ae}) \times A} \quad (23)$$

where α_c and α_r respectively denote the convective and radiative heat loss coefficients, and T_{ai} , T_{ae} , T_{si} , and T_{refl} denote the internal air, external air, internal surface, and reflected surface temperature of area A_i , respectively. Moreover, A denotes the area of the entire wall which is the summation of all A_i s.

If the values for external heat transfer coefficient (h_{ce}) are available, the U-value of an external wall surface can be quantified using the following equation [122, 131] :

$$U = \frac{h_{ce} \times A_i \times (T_{ai} - T_{si})}{A \times (T_{ai} - T_{ae})} \quad (24)$$

According to Stefan-Boltzmann law, the radiative heat varies with the fourth power of temperature difference [151]. Madding et al. replaced the radiative coefficient α_r in Eq. 23 by $4^\epsilon \sigma T_m^3$ and introduced the following equation, which contains the radiative term according to the Stefan-Boltzmann law:

$$U = \frac{4^\epsilon \sigma T_m^3 (T_{si} - T_{refl}) + \alpha_c (T_{si} - T_{ai})}{T_{ai} - T_{ae}} \quad (25)$$

where $T_m = \frac{T_s + T_{refl}}{2}$, denotes the mean temperature. ϵ and σ denote the emissivity and Stefan-Boltzmann constant, respectively. Moreover, the reflective temperature is subtracted from the surface temperature in this equation. The emissivity constant was set between 0.95 and 1.00 [126]. The convective coefficient α_c depends on various factors, including the height of the wall and temperature difference, and is given by the following equation

$$\alpha_c = c_1 \frac{(T_{si} - T_{ai})^{\frac{1}{4}}}{L} \quad (26)$$

where L is the height of the wall and the value of c_1 varies from 1.31 to 1.42. A similar equation is used by Marshall et al. [141] where the mean temperature is replaced by surface temperature. Ham et al. have given similar equation in [135, 127, 134], where fourth power of reflected temperature is subtracted from fourth power of surface temperature as given by

$$U = \frac{4^\epsilon \sigma (T_s^4 - T_{refl}^4) + \alpha_c (T_s - T_{ai})}{T_{ai} - T_{ae}} \quad (27)$$

where T_s denotes the surface temperature.

Tzifa et al. [138] suggested that if the reflected temperature is not available, it can be replaced by the air temperature in Eq. 27. The internal (α_{ci}) and external (α_{ce}) convective coefficients are considered to estimate the U-value in [98] as given by

$$U = \frac{1}{\frac{1}{\alpha_{ci}} + \frac{T_{ai} - T_{ae}}{4\epsilon\sigma(T_s^4 - T_{refl}^4) + \alpha_c(T_s - T_{ai})} + \frac{1}{\alpha_{ce}}} \quad (28)$$

In order to determine the convective heat transfer coefficient α_c , the Rayleigh number R_a , Prandtl number P_r , height of the wall L , and the thermal conductivity of the fluid k_c , are used in [140] as follows,

$$U = \frac{\epsilon\sigma(T_{refl}^4 - T_{si}^4) + \frac{k_c}{L} \left[0.825 + 0.325R_a^{\frac{1}{6}} \right]^2 (T_{ai} - T_{si})}{T_{ai} - T_{ae}} \quad (29)$$

If the fluid is air, then the value of k_c is $0.025 \text{ W m}^{-1} \text{ K}^{-1}$ when the temperature is between 20°C to 25°C . The U-value estimation for the external surface is carried out using the following equation, where the wind velocity is considered [125, 152, 139]

$$.U = \frac{\epsilon\sigma(T_{se}^4 - T_{ae}^4) + 3.805v(T_{se} - T_{ae})}{T_{ai} - T_{ae}}. \quad (30)$$

where v is the velocity of external wind. The radiative heat component is similar to Stefan-Boltzmann equation [151] and the convective term is derived from Jargon's formulae [153]. If HFM is available, the estimation of U-value is straight forward and can be done as follows [122]

$$U = \frac{\Delta Q}{t_{ae} - t_{ai}} \quad (31)$$

where Q is estimated using an HFM. The U-value can also be estimated from the thickness and thermal conductivity [154] as given below.

$$U = \frac{1}{\frac{1}{h_{si}} + \frac{1}{h_{se}} + \sum_{k=1}^n \frac{d_k}{\lambda_k}} \quad (32)$$

Table 7. Performance indices

Performance Index	Duration	Building details	Indoor setup	Reference
	1920 h	NA	Indoor temp set at 25.2 C	[155]
	2190 h	Commercial hotel	25.5 C for summer, 20.5 C for winter	[156]
	5880 h (max)	40-storey building	25.5 C for cooling, 21 C for heating	[157], [158], [159]
OTTV	NA	40-storey building	25.5 C for cooling, 22 C for heating	[160]

	NA	Single compartment building	25 C	[161], [162]
	34 yrs	39092 buildings	NA	[163]
	1 yr	1-storey building	NA	[164]
	1 yr	Multi-storey	NA	[165]
	1 yr	32-storey office building	Cooling: 26 °C, Heating: 20 °C	[2]
PAL	1 yr	Multi-storey	NA	[165]
	1 yr	32-storey office building	Cooling: 26 °C, Heating: 20 °C	[2]
OBEM	1 yr	Multi-storey	NA	[165]
ENVLOAD	1 yr	Multi-storey	NA	[165]
	NA	13-storey	NA	[166]

Table 8. Guidelines to capture UAS-based thermal images

Factor	Recommendation
Temperature difference	Internal and external wall temperature difference must be atleast 10 °C
Distance	Distance from IR camera to the wall surface should be atleast 5-15m
Solar radiation	Avoid all source of solar radiation, preferable time for thermal image capturing is dawn or dusk
Angle	IR camera must be placed at an angle less than 60 ° to the surface
Wind speed	The wind speed must be less than 5m/s between camera and inspected wall
Number of images	Atleast 40 images per position should be taken
Ambient temperature & humidity	Ambient temperature should ideally be below 35 °C and humidity below 80%

Here, d_k is the thickness, and λ_k is the thermal conductivity for each layer, and h_{si} and h_{se} are internal and external surface heat transfer coefficients, respectively.

3.7. Performance Indices

Performance indices (such as Overall Thermal Transfer Value (OTTV), Envload index, Perimeter Annual Load (PAL), Office Building envelope Energy performance and configuration Model (OBEM) index) of a building, as listed in Table 7, show the overall thermal (or heat loss) performance and provide architects valuable insights for innovative building designs [167]. The American Society of Heating, Refrigerating, and Air Conditioning Engineers (ASHRAE) defines the OTTV as a measure of average heat transfer into the building over its building envelope [168, 169]. This metric was first introduced by ASHRAE in Standard 90-75 [169] and is defined as “the maximum thermal transfer permissible into the building through its walls or roof, due to solar heat gain and outdoor–indoor temperature difference”. The OTTV can be estimated for external walls and for roofs by using the two equations as follow

$$\begin{aligned} OTTV_w = & \left(U_w \times A_w \times TD_{EQ} \right) + \left(A_f \times SF \times SC \right) \\ & + \left(U_f \times A_f \times \Delta T \right) \end{aligned} \quad (33)$$

$$\begin{aligned} OTTV_r = & \left(\left(U_r \times A_r \times TD_{EQ} \right) + \left(434.7 \times A_s \times SC \right) \right. \\ & \left. + \left(U_s \times A_s \times \Delta T \right) \right) \end{aligned} \quad (34)$$

where $OTTV_w$ and $OTTV_r$ respectively denotes the OTTV of an opaque part of wall and roof (in W/m²); U_w , U_f , U_r , and U_s denote the thermal transmittance of opaque part of wall, fenestration, opaque part of roof, and skylight, respectively (in $W / m^2 - C$); A_w , A_f , A_r and A_s respectively denotes the area of the opaque part of a wall, a fenestration, the opaque part of a roof and a skylight, respectively (in m^2); TD_{EQ} denotes the (inside and outside) temperature difference for the opaque part of a wall (or roof) (in C); SC denotes the shading coefficient of the fenestration (or skylight); SF denotes the solar factor (in W / m^2); DT denotes the temperature difference between exterior and interior building environment; ΔT denotes the temperature difference between exterior and interior design conditions.

The PAL was first introduced by Japan which measures the total annual heating and cooling requirement in perimeter of the building for unit area [170, 171]. The PAL is defined as follows

$$\begin{aligned} PAL = & (\text{Annual thermal load of the inside perimeter} \\ & \text{zone (MJ / year)}) / (\text{Total floor area of the} \\ & \text{inside ambient space of each floor} (m^2)) \end{aligned} \quad (35)$$

The *Envload* is a similar coefficient and used to estimate the cooling requirement for unit building area, and is defined as follows

$$ENVLOAD = a_0 + a_1 + \frac{\sum_{i=1}^n A_i \times K_i \times U_i \times IH_i}{A_{en}} \quad (36)$$

where a_0 and a_1 are the constants. A_i denotes the area of the i^{th} window (m^2); K denotes the modified factor for exterior shading devices; U_i denotes the heat transmittance of i^{th} window glass; IH is the annual solar radiation (kWh/m²); and A_{en} is the total area of the building envelope (m²). The OBEM is similar to ENVLOAD but applicable to office buildings as follows [165]

$$OBEM = -20370 + 2.010 \times G + 0.033 \times \left(\sum_i T_i \times L_i \times DH \right)$$

$$+ 1.079 \times \left(\sum_k^4 \sum_i^{T_i} M k_i \times IH_k \right) \quad (37)$$

where G , L_i , T_i , and DH respectively denotes annual indoor heat gain, $W - h / m^2 yr$, heat loss coefficient of building envelope in the i^{th} sector, $W / m^2 K$, sectors number of the building envelope, and DH denotes annual degree-hours based on monthly average temperature (298 K), $K - h / yr$. Moreover, DH and IH_k are affected by the building orientation and location, where IH_k and MK_i denotes the isolation-hours ($W - h / m^2 - yr$) and isolation gain coefficient on k^{th} orientation and i^{th} sector of the building.

The quantitative assessment of thermal performance depends on various factors including (i) layout or the structure of the building, (ii) type of material and its thermal properties, (iii) amount of water content or moisture present in the materials, (iv) age of the materials, and (v) alignment of different materials to form a complex structure of the building [34, 108].

The IR measurements need to be taken in the absence of solar radiation or when it has the least effect such as during dawn or cloudy weather [172, 84]. Ideally, the temperature difference is maintained as 10-15 K between internal and external environment [123]. This can be adjusted up to 7-16K [123] while maintaining accuracy. Table 8 shows the list of recommendations for thermal image capturing. The equations that estimate U-value consists of two components, (i) radiative and (ii) convective components (see Eq. 25,27,43). The radiative term is obtained using Stefan-Boltzmann equation. The convective term is different in various estimation techniques. In order to capture the convective component, the wind velocity is measured using an anemometer [125]. The convective component can also contain the length of the wall (see Eq. 25, 27). In [63, 136, 125, 3, 123], Hygrometers are used to measure the water vapour content in [139, 140].

The emissivity of the surface can be obtained from the data-sheet or using black tape [33, 122, 137]. Use of black tape requires additional efforts compared to using a data-sheet. In this method, the temperature of the material is measured adding a black tape and setting emissivity to 0.95. The emissivity that offers the same temperature of the surface after removing the black tape is the emissivity of the surface. The aluminum foil or mirrors are used to measure the reflected temperature [33, 121, 122, 137, 139, 123].

Assessment of the glazing system (or windows) is difficult compared to the other elements in a building. Glass is opaque in the long wave IR field and its thermal performance assessment using IR camera is difficult due to its high (almost 1.0) emissivity and can result in measurement errors [173, 44, 115, 174].

Reflexive properties of the surrounding objects [175] and effect of air temperature [175] can also increase the measurement inaccuracies. In order to avoid these errors, the following corrective measures are proposed in [174, 173, 175]: (1) use of internal qualitative measurement (or indoor, controlled environment) instead of external qualitative measurement; (2) use of high emissivity materials like black tape and electric tape, as reference to estimate emissivity; and (3) maintaining a temperature difference of 15 °C between the inside and outside walls [174, 173, 175]. These measurements are generally performed in the absence of solar radiation or when it has the least effect such as during dawn or cloudy weather [172, 34, 108, 109, 18, 176]. Additional techniques were used to improve the measurement accuracy such as (1) sonic trials to estimate the overall wall density [84]; (2) ultrasonic devices to assess the structural defects [177, 178]; (3) gravimetric tests to determine the water content present in the wall [101]; (4) chemical investigation to identify the chemical components present in the wall [61, 179, 180, 181].

Table 9. Building datasets, window, and wall properties

Building Name	Image details	Capturing	Weather Details	Wind ow prope	Wall Properties

							W	W			
	# images	Date	Time	Avg Temp (C)	Humidity (%)	Avg wind speed (mph)		Avg surface temp (thermocouple)	Emissivity	Surface type	Material type
	2480	9th Oct, 2019	06:30 - 07:30 hrs	NA	79	7		NA			Brick
Twamley Hall	878	17th Mar, 2020	07:00- 20:00 hrs	21.2	69	10	Singl e pane glass	9.73	0.75	Rough	Brick
	906	8th Oct, 2019	18:55 - 19:55 hrs	18.0	55	9		14.9			Brick
Museum of Art	710	17th Mar, 2020	07:00- 20:00 hrs	21.2	69	10	Double pane glass	2.56	0.75	Rough	Brick

Figure 5. Database layer

4. Data-driven Three-layered Framework

There are several methods for thermal assessment of buildings discussed in the literature. However, infrared thermal imagery seems to be promising due to its extensive features, high performance abilities, and relatively cheaper cost. Nevertheless, some intricacies exist in IRT imagery and requires a deeper understanding of different parameters that could influence the measurement results. IRT requires a knowledge of construction materials and thermodynamic properties of building elements, various environmental parameters, and distance between camera and test specimen.

However, the thermal images must be pre-processed and automated before collecting any meaningful information. This includes removal of unwanted background objects and detection of the inspected specimen such as window, door, and wall, etc. However, limited contribution exists in the current literature in terms of automating the methods for background removal, object detection and U-value estimation. This lack of contribution motivates us to propose a fully automated method for U-value

estimation of a building and its elements. Fig. 6 shows a data-driven approach for thermal performance assessment of building envelope.

Figure 6. Data-driven approach for thermal performance assessment

The raw thermal imagery captured from various sources (E.g. aerial/ground measurement) are stored in a data repository (database layer). The images are fed into a pre-processing and automation layer, where a series of background elimination steps are undertaken, and the important features from the thermal images are extracted (refer Fig. 6); different elements of a building such as doors, roofs, facades, beams, and windows, are annotated and this dataset is used for training the machine learning models for object detection. Finally, the heat loss (U-value) of a building elements/envelope is quantified in the evaluation layer while considering the influential parameters (emissivity and reflected temperature).

Figure 7. Machine learning workflow for U-value estimation

4.1. Database Layer

Thermal images of different buildings of University of North Dakota (UND) campus were collected to form a dataset of approximately 5000 thermal images (refer Table 9 and Fig. 5). These images were collected using a drone equipped with a Mirage 650 OGI sensor on different days. Initial datasets for machine learning and U-value estimation consisted of FLIR images but a gradual shift was made to using OGI images (primarily for U-value estimations) due to its higher precision and consistency in measurements. A HOBO sensor was used to collect the inside and outside building ambient air temperatures. Moreover, thermocouples were used to verify the surface temperatures obtained from thermal images. The environmental parameters (such as wind speed, air temperature) were obtained from Wunderground website [182]. The database layer also contains the building energy consumption data, which can be used further to validate the total heat-loss obtained using thermal images. Moreover, the database layer is responsible for housing all of the relevant data for training and testing our models. Further verification can be obtained using the Computer Aided Design (CAD) models. The database layer stores the raw and annotated datasets, models and their iterations, logs, and evaluation results. For redundancy purposes, copies of the models and dataset are stored on the High-performance Computing (HPC) clusters and Supervisely servers [183].

4.2. Pre-processing and Automation Layer

The pre-processing and automation layer is responsible for tasks such as background elimination, object detection, and instance classification that are required to extract meaningful insights from thermal imagery.

4.2.1. Background Elimination

Presence of unwanted objects such as trees, grounds, sky etc. can interfere with the heat-loss estimation of the building. The authors of this paper have already carried out work on the background elimination of thermal images using Canny based Edge Detection (CED) and Dominant Color Isolation (DCI) [97]. The CED method uses first-order directional Gaussian derivatives to find edges by linking high-gradient pixels. This method extracts useful structural information from the gray scale images. This technique performs well when the objects are visually distinctive, such as the building wall and the sky (refer Fig. 8), but fails to perform when indistinct objects, like trees, windows, and doors, are present. Image 118 is an example when the edge detection method produces bad results. Dominant Color Masking (DCM) technique separates the image into DCMs and masks the remaining channels by binarizing the image. This technique computes the euclidean distance between colors in LAB Color space, where L is the lightness or approximate luminance, A is the first color parameter, green (negative) to magenta (positive) and B is the second color parameter, blue (negative) to yellow (positive) forming the vector L,A,B, and A, B are in the range of ± 1 . The Dominant Color Masking (DCM) performs relatively better than CED when indistinct objects are present in the image.

Figure 8. Comparison of various methods

Table 10. Comparison of accuracy of background elimination techniques

Image #	False positives (%)	False negatives (%)	Total error (%)
Canny Edge Detection			
192	$\frac{370}{327680} = 0.11$	$\frac{44654}{327680} = 13.63$	$\frac{45024}{327680} = 13.74$
118	$\frac{2}{327680} = 0.0$		
Dominant Color Isolation			
192	$\frac{13620}{327680} = 4.16$	$\frac{23555}{327680} = 7.19$	$\frac{37175}{327680} = 11.34$
118	$\frac{2316}{327680} = 0.71$	$\frac{90030}{327680} = 27.48$	

The following metrics were used to evaluate the performance of these two approaches:

$$\text{False positives} = \frac{\text{Pixels incorrectly removed}}{\text{Total number of pixels}} \quad (38)$$

$$\text{False negatives} = \frac{\text{Pixels incorrectly remain}}{\text{Total number of pixels}} \quad (39)$$

The accuracy of the CED and DCI methods in terms of these indices is compared in Table 10. CED produces much fewer false positives (FP) as compared to the number of false negatives (FN) for image 192. It also shows that DCI produces fewer FPs than FNs in all three cases. It can be observed that the total error rates using DCI on Image 192 was slightly lower than the edge detection method, and the number of false positives was lower using edge detection. Moreover, DCI has more FPs but fewer FNs. In summary, DCI performs better than canny edge detection (Table 10).

4.2.2. Instance Segmentation

In order to accurately quantify the heat-loss, we need to detect different elements (such as doors, windows, walls etc.) of a building. In this work, we use machine learning based object detection techniques to accurately identify building elements. Moreover, after detecting the object it is necessary to identify the corresponding pixels in a thermal image. In order to achieve pixel-by-pixel classification, we needed a machine learning model that is capable of accomplishing instance segmentation. Instance segmentation is the combination of object detection, classifying objects and localizing with bounding boxes, and semantic segmentation. The semantic segmentation classifies objects with a pixel level association. Convolution Neural Network (CNN) is a type of Neural Network that performs extremely well for segmentation [184].

Mask R-CNN [185] is a supervised learning model, where the neural network learns from manually (human) annotated objects with the desired classes and tags. In order to organize the tremendous amount of data generated during annotations, training, and testing phases, we used a web-based platform called Supervisely [183]. The Supervisely web-portal offers the ability for training (e.g. by providing the model name, labeled dataset, and hyper-parameters) and testing several models with very few interactions. Supervisely provides a convenient Data Transformation Language (DTL) to easily manipulate datasets. We used the DTL feature to augment and split the data set into training and validation sets.

Figure 7 demonstrates an end-to-end pipeline starting from user requests to U-value evaluation. First, the user requests a task to be performed on a dataset which gets sent to the database layer. This layer keeps a running track of all tasks requested. If the user requests a model to be trained, the task gets relayed to the Supervisely platform. This platform keeps track of all the model weights and logs. If the requested task is a ‘testing’, the automation layer gets triggered, then the model metrics such as mean average precision (mAP) and mean intersection over union (mIoU) are computed. These results are then uploaded to the supervisely platform. Wall temperature is collected from the CSV’s, the building dimensions from architectural blueprints, weather data from wunderground [182] database, and object coordinates from the JSON file. These external parameters are brought in for the U-value assessment in the evaluation layer.

4.3. Evaluation Layer

The evaluation layer consists of testing the Mask R-CNN model on a particular dataset, and extracting the ROI’s to compute the relevant heat-loss or U-values with respect to the object identified by the model.

$$Precision = \frac{TP}{(TP + FP)} \quad (40)$$

$$Recall = \frac{TP}{(TP + FN)} \quad (41)$$

The *Precision* denotes the accuracy of the predictions and expressed as a percentage of True Positives (TP) and Total Positives which is the summation of TP and False Positives (FP). Whereas, *Recall* is estimated as the ratio of TP and, FP and False Negatives (FN).

$$IoU = \frac{\text{Area of overlap}}{\text{Area of union}} \quad (42)$$

Intersection over union (IoU) is a widely used metric to evaluate semantic segmentation, and image segmentation, applications [186]. The IoU denotes a percentage of pixels that overlap over between the model’s annotation and ground truth over all of the pixels occupied by both of the annotations.

5. Results and Discussion

5.1. Instance Segmentation

In order to train the thermal images, a polygon tool (provided by Supervisely [183]) was used for annotation to mark the silhouette of the object of interest (facades, windows, and roofs), and then subsequently tagged by its name. These annotations are converted into a JSON (JavaScript Object Notation) format that is readable by the Mask R-CNN model. The overall structure of JSON file consists of each identified object, classTitles, followed by the co-ordinates populated by each of these objects. The Mask R-CNN model was trained on the Microsoft COCO dataset. This dataset consists of 1.5 million object instances with 80 object categories. Due to initial smaller size of our dataset, we chose to employ transfer-learning rather than training our model on our own custom dataset. In transfer learning, the pre-trained weights of the COCO dataset could be used as initialization weights and the model is retrained and re-purposed. One problem of small datasets is over-fitting, and to overcome this issue, data augmentation was applied. Using the DTL API, three different types of transformations were applied: a vertical flip transformation is applied first, followed by a multiply transformation that makes an exact copy of the image, and a crop filter that was added with a minimum crop width and height of 70% with a maximum crop of 90%. The three augmentations multiplied the dataset, on average, by a factor of 22 (over 100,000 images in the augmented dataset).

Table 11. Mask R-CNN model training parameters

Model	Learning	Input	Number of GPU's	Epochs
Name	Rate	Resolution		
	0.00001	256X256	1	200
	0.00001	256X256	1	5
	0.00001	256X256	1	200
	0.00001	256X256	1	100
	0.00001	256X256	1	100
	0.00001	256X256	1	50
	0.00001	256X256	1	100
	0.0001	256X256	1	10
	0.0001	256X256	1	10
Mask RCNN	0.001	256X256	1	50

The training of the Mask R-CNN model was accomplished on a High Performance Computer (HPC) with NVidia RTX 2080Ti graphics card. Supervisely provides a Docker image that links the HPC cluster to the Web API. We are able to run the specified model and dataset on the HPC while uploading results to Supervisely as specified by the configuration file. Within this configuration file, the hyper-parameters—such as learning rate, input resolution, number of GPU's, and epochs—are specified. These hyper-parameters were held constant throughout each training session, except for learning rate, as illustrated in Table 11. However, the optimal number of epochs to train the models is challenging to determine. One way to determine the number of epochs required is to observe the loss function which will eventually start to converge on a value. The input dimensions for the model were set to 256x256 and the batch size was set to train on one image and validate on one image.

Table 12. Mask R-CNN evaluation metrics

Object	AP ^{0.25}	AP ^{0.50}	AP ^{0.75}	IoU
Window	0.68	0.67	0.37	0.05
Façade	0.58	0.46	0.27	0.50
Average	0.63	0.56	0.32	0.46

In order to evaluate the Mask R-CNN model, we built our test dataset which consists of 54 FLIR images and 102 OGI images. At the end of each training session the best performing model's (lowest loss) weights are saved in a .h5 file and used for inferencing. The coordinates calculated by the mask are then saved within a JSON file.

Figure 9. U-value analysis of windows and walls (March 17th, 2020 morning)

The Mask R-CNN model was evaluated on its accuracy of object detection and mask (refer Table 12). The model was trained on FLIR images and tested on a dataset containing both 54 FLIR and 102 OGI images. Overall the average precision, at confidence level of 0.50, for windows is 0.67 and facade is 0.46 with a mean average precision of 0.56. The detection of windows out performs the detection of facades, but the accuracy of the mask for windows is low. When evaluating the mask accuracy of facades we are able to achieve 0.50.

5.2. Heat Loss Estimation via Surface temperature analysis

Figure 10. Twamley window 1: Single pane (temperature/U-value) captured on October 9, 2019

Figure 11. Museum window 1: Double pane (temperature/U-value) captured on October 8, 2019

The raw thermal images were analyzed using IR Flash Pro software to extract the temperature data. For an accurate U-value estimation, we used the manual annotated images instead of the direct software annotation from the Mask R-CNN model. This is due to the fact that there is still not a 100% detection accuracy on the masks or instances. The preliminary results analyzed buildings from direct annotated U values from Mask R-CNN are yet closer to manually done annotated images. For reliability and completeness of the estimation of surface temperature estimation, we used actual surface temperature for the entire objects such as windows, facades, walls and roofs. The U-value trend for the single-pane and double-pane windows are shown in Fig. 9. The Twamley Hall building windows at the UND campus are single-pane windows, whereas the windows at the Musuem are of double-pane. The double pane windows are more efficient than single pane windows in insulating the heat-flow. The results correlates with this assessment as U-values correspond to single pane are higher than double pane windows (refer Fig. 9). The average temperature for single-pane and double-pane windows are 12.85 and 9.21 °C, respectively (refer Fig. 10 and Fig. 11).

Table 13. Twamley region-wise average temperature analysis

	Left	Middle	Right	Avg
Upper	14.56	14.65	17.75	15.65
Middle	11.73	11.71	11.73	11.72
Bottom	14.29	14.27	15.23	14.60
Avg	13.53	13.54	14.90	–

Table 14. Museum region-wise average wall temperature analysis

	Left	Middle	Right	Avg
Upper	9.02	8.96	8.72	8.9
Middle	8.38	8.59	11.75	9.57
Bottom	7.58	9.09	15.8	10.82
Avg	8.33	8.88	12.09	–

Table 15. Museum U-value estimation (evening) on October 8, 2019

		Temperature Analysis						U-value Analysis				ASHR AE	
		Surface temperature											
		# images	Ma x	Mi n	Avg	Thermocou ple	External Air	U ₁	U ₂	U ₃	U _c		
Wind	w 1	26	10. 0	6.7 8	9.21	temperatu re	temperatu re	0.3 3	0.1 1	0.1 0	0.1 8	0.35	

Window (all)	339	13.6	9.5	11.89			0.41	0.14	0.14	0.23	0.35
Wall 1	435	13.4	6.5	9.3			0.84	0.69	0.26	0.26	0.085
Roof	184	13.9	5.14	7.0	18 C	15 C	0	0	0	0	0.04

Table 16. Twamley U-value estimation (morning), October 9, 2019

		Temperature Analysis						U-value Analysis				
		Surface temperature							U-value Analysis			
Building elements	# images	Max	Min	Avg	Thermocouple temperature	Air temperature		U1	U2	U3	Uc	ASHRAE
Window 1	26	17.84	13.49	14.55				0.77	0.74	0.71	0.74	0.95
Windows (all)	1333	25.25	4.23	12.93				1.36	0.48	0.46	0.77	0.95
Wall 1	1396	24.18	4.30	12.85				0.71	0.69	0.66	0.69	0.085
Roof	174	2.64	0.26	1.3	7.9 C	6.3		0	0	0	0	0.04

Table 17. Twamley U-value estimation (morning) on March 17, 2020

		Temperature Analysis						U-value Analysis				
		Surface temperature							U-value Analysis			
Building	# images	Max	Min	Avg	Thermocouple temperature	Air temperature		U1	U2	U3	Uc	ASHRAE
Window 1	5	-2.90	-5.89	-4.54				0.84	0.26	0.25	0.45	
Windows in Face 1	334	-3.80	-5.53	-4.88				0.82	0.26	0.25	0.44	
Windows in Face 2	59	-3.87	-5.69	-5.12				0.80	0.25	0.24	0.43	
Windows	87	-	-	-				0.8	0.2	0.2	0.4	

in Face 3		3.28	5.7 3	4.9 8			1	5	4	4	
Windows in Face 4	288	- 5.54	- 6.6 0	- 6.1 4			0.6 9	0.2 1	0.2 1	0.3 7	
All Windows	779	- 0.95	- 6.9 9	- 5.4 0	NA		0.7 7	0.2 4	0.2 3	0.4 1	0.95
Wall 1	114	- 3.92	- 5.5 8	- 4.9 4			0.6 8	0.2 2	0.2 1	0.3 7	
Wall 2	38	- 2.91	- 5.7 9	- 4.7 1			0.6 7	0.2 1	0.2 0	0.3 6	
Wall 3	51	- 3.26	- 5.6 5	- 4.9 1			0.6 6	0.2 1	0.2 0	0.3 6	
Wall 4	52	- 5.64	- 6.6 0	- 6.1 7			0.5 5	0.1 7	0.1 6	0.2 9	
Walls	262	- 0.76	- 7.0 7	- 5.2 4	-2		0.6 4	0.2 0	0.1 9	0.3 5	0.085
Roof	62	15.1 2	- 7.7 1	- 4.8 7	NA	-7.0 C	0.8 8	0.2 8	0.2 7	0.4 7	0.04

Table 18: Twamley U-value estimation (afternoon) on March 17, 2020

		Temperature Analysis											
		Surface temperature					U-value Analysis						
Building	# images	Max	Min	Avg	Thermocouple	Air temperature	U1	U2	U3	Uc	ASHRAE		
											AE		
Window 1	11	54.3 2	12.5 0	25.0 9			3.0 4	1.4 8	1.3 9	1.9 5			
Windows in Face 1	295	60.1 8	12.1 1	28.3 5			3.5 1	1.7 5	1.5 5	2.2 8			
Windows in Face 2	79	52.1 8	1.28 3	18.2 3			2.0 9	1.0 1	0.9 2	1.3 4			
Windows	84	54.0	-	3.82			0.0	0.0	0.0	0.0			

in Face 3		1	0.19				9	4	3	5	
Windows in Face 4	200	38.0 5	- 0.57	9.58			1.0 9	0.5	0.4 6	0.6 8	
All Windows	723	60.1 8	- 0.57	18.1 9	NA		2.0 9	1.0 2	0.9 2	1.3 4	0.95
Wall 1	43	60.1 8	9.01	33.8 3			5.2 0	3.0 9	2.5 5	3.6 2	
Wall 2	34	60.1 8	- 7.26	17.6 9			3.0 6	1.6 7	1.4 4	2.0 6	
Wall 3	62	54.6 8	- 0.19	4.35			0.8 0	0.3 6	0.3 4	0.5 0	
Wall 4	55	57.1 2	- 1.11	10.1 3			2.0 3	1	0.9 1	1.3 3	
All Walls	270	60.1 8	- 7.20	18.2 4	-23.7 C	3.1 C	3.9 0	2.1 8	1.8 5	2.6 4	0.085
Roof	62	60.0 4	- 1.40	19.9 0	NA	NA	2.3 7	1.2 6	1.0 9	1.5 7	0.04

In order to capture the temperature profile of different sections of the wall, we show the average temperature of corresponding sections in Table 13 and Table 14. Table 13 shows that the upper-right section of Twamley encounters maximum heat loss, whereas Table 14 shows the bottom-right section of the Museum building encounters maximum heat loss. The emissivity, outside and inside air temperature, and wind velocities were captured to accurately estimate the U-values. The outdoor temperature was obtained from the HOBO sensor embedded in the drone. A weather data site called Wunderground was used [182] to gather wind velocity. Following equations are used to quantify the heat loss transmittance coefficient.

$$U_1 = \frac{\epsilon \sigma (T_{se}^4 - T_{ae}^4) + 3.805 v (T_{se} - T_{ae})}{T_{ai} - T_{ae}} \quad (43)$$

$$U_2 = \frac{4\epsilon \sigma T_s^3 (T_{si} - T_{refl}) + \alpha_c (T_{si} - T_{ai})}{T_{ai} - T_{ae}} \quad (44)$$

$$U_3 = \frac{4\epsilon \sigma T_m^3 (T_{si} - T_{refl}) + \alpha_c (T_{si} - T_{ai})}{T_{ai} - T_{ae}} \quad (45)$$

$$U_c = \frac{U_1 + U_2 + U_3}{3} \quad (46)$$

where v is the velocity of external wind, T_s is the surface temperature, $T_m = \frac{T_s + T_{refl}}{2}$ denotes the mean

temperature, $\alpha_c = c_1 \frac{(T_{si} - T_{ai})^{\frac{1}{4}}}{L}$ denotes the convective heat transmittance coefficient, and U_c denotes the

cumulative U-value. We set the Stefan-Boltzmann constant $\sigma = 5.67 \times 10^{-8} \text{ W m}^{-2} \text{ K}^{-4}$ and emissivity $\epsilon =$

0.75 for walls and 1.0 for windows. The surface temperatures (T_{si} and T_{se}) were obtained using the thermal images. The building height information is noted from the architectural diagram.

Table 19. Twamley U-value estimation (evening) on March 17, 2020

		Temperature Analysis						U-value Analysis						
		Surface temperature							U-value Analysis					
Building	# images	Max	Min	Avg	Thermocouple	Thermocouple	Air temperature	U1	U2	U3	Uc	ASHRAE		
Window 1	11	2.38	-1.19	-0.67				0.71	0.15	0.15	0.33			
Windows in Face 1	279	3.16	-1.26	-0.29				0.78	0.16	0.16	0.37			
Windows in Face 2	33	7.29	-0.81	1.02				1.03	0.22	0.22	0.49			
Windows in Face 3	23	4.35	-0.98	0.14				0.86	0.18	0.18	0.41			
Windows in Face 4	167	2.72	-1.31	-0.61				0.72	0.15	0.15	0.34			
Windows in Face 5	132	3.51	-1.89	-1.09				0.63	0.13	0.13	0.30			
All Windows	645	4.21	-1.25	-0.16	NA			0.80	0.17	0.17	0.38	0.95		
Wall 1	106	2.87	-1.24	-0.20				1.42	0.32	0.30	0.68			
Wall 2	35	6.60	-0.76	2.03				1.74	0.40	0.38	0.84			
Wall 3	13	4.77	-0.98	0.48				1.74	0.40	0.38	0.84			
Wall 4	68	3.95	-1.34	0.04				1.40	0.31	0.30	0.67			

			9								
Wall 5	70	3.2 2	- 1.9 2	- 1.0 6			1.4 3	0.3 2	0.3 1	0.6 9	
All Walls	292	4.2 8	- 1.2 6	0.2 6	-7.5 C	-4.4 C	1.5 5	0.3 5	0.3 4	0.7 4	0.085
Roof	82	2.4 8	- 3.8 0	- 2.1 1	NA	NA	0.4 3	0.0 9	0.0 9	0.2 0	0.04

Table 20. Museum U-value estimation (morning) on March 17, 2020

		Temperature Analysis										
		Surface temperature					U-value Analysis					
Building	# images	Max	Min	Avg	Thermocouple	Air	U1	U2	U3	Uc	ASHRAE	
						temperature						
Window 1	28	-1.6	-5.9	-4		-11 C	0.5	0.196	0.19	0.29		
Windows in Face 1	166	0.36	-6.4	-5.1		-11 C	0.42	0.16	0.15	0.24		
Windows in Face 2	155	3	-7	-4.1		-11 C	0.49	0.19	0.18	0.29		
All Windows	321	3	-7	-4.6	NA	-11 C	0.46	0.177	0.172	0.27	0.35	
Wall 1	107	6.1	-6.8	-5.4		-11 C	0.33	0.130	0.126	0.1		
Wall 2	126	3	-7	-4.3		-11 C	0.34	0.133	0.13	0.2		
All Walls	233	6.1	-7	-4.7	-4.7 C	-11 C	0.34	0.133	0.130	0.20	0.085	
Roof	121	5.5	-7.9	-6.3	NA	NA	0.33	0.41	0.12	0.12	0.04	

Table 21. Museum U-value estimation (afternoon) on March 17, 2020

		Temperature Analysis										
		Surface temperature							U-value Analysis			
Building	#	Max	Min	Avg	Thermocouple	Air	U1	U2	U3	Uc	ASHR	
Building A	101	72.5	68.0	70.2	TC-A1	71.0	0.15	0.16	0.17	0.18	0.19	ASHR-101

Building Elements	# images	x	n		Thermocouple	Air temperature					AE
					temperature						
Window 1	18	14.51	2.89	7.02		3.1 C	0.5	0.196	0.19	0.29	
Windows in Face 1	217	23.49	2.32	7.03		3.1 C	0.62	0.254	0.24	0.37	
Windows in Face 2	184	30.6	0.3	7.09		3.1 C	0.63	0.286	0.26	0.39	
All Windows	402	60.18	0.3	7.06	NA	3.1 C	0.62	0.265	0.25	0.38	0.35
Wall 1	114	19.41	2.32	7.54		3.1 C	0.96	0.398	0.38	0.58	
Wall 2	98	60.18	-1.7	8.46		3.1 C	1.57	0.728	0.68	1	
All Walls	213	60.18	-1.7	7.97	20.0 C	3.1 C	1.25	0.542	0.52	0.77	0.085
Roof	38	60.18	-2.24	12.47	NA	3.1 C	1.52	0.737	0.67	0.97	0.04

Table 22. Museum U-value estimation (evening) on March 17, 2020

		Temperature Analysis										
		Surface temperature						U-value Analysis				
Building	# images	Max	Min	Avg	Thermocouple	temperature	Air	U1	U2	U3	Uc	ASHRAE
Elements							temperature					AE
Window 1	29	-2.7	-2.2	0.5		-4 C	0.41	0.162	0.158	0.24		
Windows in Face 1	128	8.6	-3	0.1		-4 C	0.38	0.14	0.14	0.22		
Windows in Face 2	136	11.5	-0.5	3.8		-4 C	0.62	0.249	0.241	0.37		
All Windows	264	11.5	-0.5	2.03	NA	-4 C	0.56	0.22	0.21	0.33	0.35	
Wall 1	115	5.1	-2.6	0.05		-4 C	0.4	0.158	0.155	0.24		
Wall 2	110	11.	-	3.9		-4 C	0.5	0.24	0.23	0.3		

		5	2.8				9			5	
All Walls	225	11. 5	- 2.8	1.9	1.2 C	-4 C	0.4 4	0.18 0	0.17 5	0.2 6	0.085
Roof	65	4.2	- 3.3	- 0.9	NA	-4 C	0.2 8	0.10 7	0.10 5	0.1 6	0.04

Tables 15, 20, 21, and 22 show the U-values (U_s , U_m , U_{avg} , U_c) and compared with the ASHRAE standard data (in BTU/hr °F ft²) for the Museum building in UND campus. These tables also contain the building element type, the total number of images analyzed, the minimum, maximum, and average surface temperatures, thermocouple temperature obtained from the building surface, and the air temperature from weather data. Similarly, Tables 16, 17, 18, and 19 show the U-values and related parameters for UND's Twamley building. The U-value results indicate that single-pane windows (i.e. Twamley building) are less efficient than the double-pane windows (i.e. Museum building). Moreover, the afternoon U-values are higher than the morning and evening U-values due to the effect of sunlight. We also noticed that the window values are more consistent with the ASHRAE standard, whereas the wall values are more consistent with the ASHRAE standard.

6. Conclusion

A detailed evaluation of heat loss measurement types, processes, and methods (e.g., both qualitative and quantitative) of IRT/non-IRT approaches are discussed. Specifically, a novel three-layered framework with an application of instance segmentation method (i.e., Mask R-CNN) was investigated. Estimations of U-value for multiple objects of buildings (e.g., facades, walls, windows, and roofs) are calculated. The U-value results show that the UAV-assisted thermal imagery-based heat-loss estimation can effectively distinguish between single and double pane windows and also consistent with the ASHRAE standards. The Twamley windows are single pane (Avg U-value: approx. 0.9), whereas the Museum windows are double pane (Avg U-value: approx. 0.3). Heat loss estimation for the walls is not consistent with the ASHRAE standard. However, the thermal imagery-based techniques are efficient to identify the old and new building walls. The U-values for the Twamley walls (old) are consistently higher than Museum walls (relatively new). Moreover, the afternoon U-values are unacceptable due to the solar irradiance effects, which confirms that surface free from any incident solar radiation is the most suitable for thermal imagery data.

7. Future Work

The future work includes (1) improving the automation of instance segmentation models and estimating surface temperatures seamlessly in real-time; (2) correlating thermal assessment of multiple UAS imagery of same building over different seasons and with energy consumption and material data of buildings and (3) hotspot detection via pixel-by-pixel analysis; (4) full automation of the data capturing process wherein building inspections can be carried out remotely with little to no human intervention by setting pre-determined flight paths [187]; (5) real-time 3D modeling (e.g., using point clouds) of the inspected building(s) through the combined use of the captured 2D thermal and color images through monocular thermography to offload post-processing computational loads; and (6) the recruitment of a ground-based vehicle to be used in tandem with a UAV that acts as a charging station for the UAV to make large-scale inspections more feasible on a single run [188].

8. Acknowledgement

The authors acknowledge the support from our collaborators such as North Dakota Department of Commerce (Award # UND0022166), SkySkopes, Inc, VPR office at the UND, university system office

for enabling acquisition of thermal images in the 11 campuses at NDUS, Michael Nord, Building Facilities Manager, and Dr. Gautham Krishnamoorthy, Professor of Chemical Engineering at the UND campus.

References

- [1] O. Kaynakli, A review of the economical and optimum thermal insulation thickness for building applications, *Renewable and Sustainable Energy Reviews* 16 (1) (2012) 415–425.
- [2] J. Lee, J. Kim, D. Song, J. Kim, C. Jang, Impact of external insulation and internal thermal density upon energy consumption of buildings in a temperate climate with four distinct seasons, *Renewable and Sustainable Energy Reviews* 75 (2017) 1081–1088.
- [3] L. Aditya, T. Mahlia, B. Rismanchi, H. Ng, M. Hasan, H. Metselaar, O. Muraza, H. Aditiya, A review on insulation materials for energy conservation in buildings, *Renewable and sustainable energy reviews* 73 (2017) 1352–1365.
- [4] S. Grammatikos, E. Kordatos, T. Matikas, C. David, A. Paipetis, Current injection phase thermography for low-velocity impact damage identification in composite laminates, *Materials & Design* 55 (2014) 429–441.
- [5] C. Ibarra Castanedo, J. M. Piau, S. Guilbert, N. P. Avdelidis, M. Genest, A. Bendada, X. P. Maldague, Comparative study of active thermography techniques for the nondestructive evaluation of honeycomb structures, *Research in Nondestructive Evaluation* 20 (1) (2009) 1–31.
- [6] N. Nazaryan, C. Campana, S. Moslehpoour, D. Shetty, Application of a he3ne infrared laser source for detection of geometrical dimensions of cracks and scratches on finished surfaces of metals, *Optics and Lasers in Engineering* 51 (12) (2013) 1360–1367.
- [7] Y. K. An, J. Yang, S. Hwang, H. Sohn, Line laser lock in thermography for instantaneous imaging of cracks in semiconductor chips, *Optics and Lasers in Engineering* 73 (2015) 128–136.
- [8] Residential energy services network (resnet). interim guidelines for thermographic inspections of buildings. resnet (2012).
- [9] American society for testing and materials (astm). standard practice for thermographic inspection of insulation installations in envelope cavities of frame buildings. west conshohocken: Astm (1997).
- [10] European committee for standardization (cen), thermal performance of buildings. qualitative detection of thermal irregularities in building envelopes, infrared method, standard en 13187, cen, brussels (1998).
- [11] International organization for standardization (iso), condition monitoring and diagnostics of machines. thermography, standard 18434, iso, geneve (2008).

- [12] American society for testing and materials (astm), standard test method for minimum resolvable temperature difference for thermal imaging systems, e 1213, astm, west conshohocken (2009).
- [13] American society for testing and materials (astm), standard test methods for measuring and compensating for emissivity using infrared imaging radiometers, e 1933, astm, west conshohocken (2005).
- [14] American society for testing and materials (astm), standard test method for minimum detectable temperature difference for thermal imaging systems, 1311, astm, west conshohocken (2004).
- [15] American society for testing and materials (astm), standard test method for measuring and compensating for reflected temperature using infrared imaging radiometers, e 1862, astm, west conshohocken (1997).
- [16] American society for testing and materials (astm), standard guide for examining electrical and mechanical equipment with infrared thermography, e 1934, astm, west conshohocken (2005).
- [17] American society for testing and materials (astm), standard practice for thermographic inspection of insulation installations in envelope cavitiesof frame buildings, c 1060 11, astm, west conshohocken (1997).
- [18] C. Pearson, Thermal imaging of building fabric, bisra guide bg39 (2011).
- [19] E. Lucchi, Applications of the infrared thermography in the energy audit of buildings: A review, Renewable and Sustainable Energy Reviews 82 (2018) 3077–3090.
- [20] H. Kayan, R. Eslampanah, F. Yeganli, M. Askar, Heat leakage detection and surveiallance using aerial thermography drone, in: 2018 26th Signal Processing and Communications Applications Conference (SIU), 2018, pp. 1–4.
- [21] A. A. Muresan, S. Attia, Energy efficiency in the romanian residential building stock: A literature review, Renewable and Sustainable Energy Reviews 74 (2017) 349–363.
- [22] B. P. I. E. (BPIE), Europeś buildings under the microscope, a country-by-country review of the energy performance of buildings (2011).
- [23] F. Ascione, N. Bianco, R. F. De Masi, G. M. Mauro, M. Musto, G. P. Vanoli, Experimental validation of a numerical code by thin film heat flux sensors for the resolution of thermal bridges in dynamic conditions, Applied energy 124 (2014) 213–222.

- [24] F. Ascione, F. Ceroni, R. F. De Masi, F. de Rossi, M. R. Pecce, Historical buildings: Multidisciplinary approach to structural/energy diagnosis and performance assessment, *Applied energy* 185 (2017) 1517–1528.
- [25] P. G. Cesaratto, M. De Carli, A measuring campaign of thermal conductance in situ and possible impacts on net energy demand in buildings, *Energy and Buildings* 59 (2013) 29–36.
- [26] J. Siviour, Experimental u-values of some house walls, *Building Services Engineering Research and Technology* 15 (1) (1994) 35–36.
- [27] E. Lucchi, *Diagnosi energetica strumentale degli edifici*, Dario Flaccovio Editore, Palermo (2012).
- [28] S. Doran, E. Kilbride, Safety and health business plan, field investigations of the thermal performance of construction elements as built (2000).
- [29] S. Rhee-Duverne, P. Baker, Research into the thermal performance of traditional brick walls, London: English Heritage (2013).
- [30] E. Lucchi, Thermal transmittance of historical stone masonries: A comparison among standard, calculated and measured data, *Energy and Buildings* 151 (2017) 393–405.
- [31] B. Abad, D. A. Borca Tasciuc, M. Martin Gonzalez, Non contact methods for thermal properties measurement, *Renewable and Sustainable Energy Reviews* 76 (2017) 1348–1370.
- [32] B. ISO et al., Building materials and products hygrothermal properties tabulated design values and procedures for determining declared and design thermal values (2007).
- [33] P. A. Fokaides, S. A. Kalogirou, Application of infrared thermography for the determination of the overall heat transfer coefficient (u value) in building envelopes, *Applied Energy* 88 (12) (2011) 4358–4365.
- [34] Residential Energy Services Network (RESNET). Interim guidelines for thermographic inspections of buildings., RESNET; 2012.
- [35] C. Koo, S. Park, T. Hong, H. S. Park, An estimation model for the heating and cooling demand of a residential building with a different envelope design using the finite element method, *Applied energy* 115 (2014) 205–215.
- [36] V. Neela, A. De, Three-dimensional heat transfer analysis of lens tm process using finite element method, *The International Journal of Advanced Manufacturing Technology* 45 (9-10) (2009) 935.
- [37] E. Grinzato, P. Bison, S. Marinetti, Monitoring of ancient buildings by the thermal method, *Journal of Cultural Heritage* 3 (1) (2002) 21–29.

- [38] N. Avdelidis, A. Moropoulou, Applications of infrared thermography for the investigation of historic structures, *Journal of Cultural Heritage* 5 (1) (2004) 119–127.
- [39] E. Barreira, R. M. Almeida, J. Delgado, Infrared thermography for assessing moisture related phenomena in building components, *Construction and building materials* 110 (2016) 251–269.
- [40] G. R. Stockton, Methodologies of finding, analyzing and prioritizing moisture problems in roofing materials using infrared thermal imaging, *IR/INFO* 2013 (2013).
- [41] S. M. Ocaña, I. C. Guerrero, I. G. Requena, Thermographic survey of two rural buildings in spain, *Energy and Buildings* 36 (6) (2004) 515–523.
- [42] M. Fox, S. Goodhew, P. De Wilde, Building defect detection: External versus internal thermography, *Building and Environment* 105 (2016) 317–331.
- [43] E. Barreira, R. M. Almeida, M. Moreira, An infrared thermography passive approach to assess the effect of leakage points in buildings, *Energy and Buildings* 140 (2017) 224–235.
- [44] T. Taylor, J. Counsell, S. Gill, Energy efficiency is more than skin deep: Improving construction quality control in new build housing using thermography, *Energy and Buildings* 66 (2013) 222–231.
- [45] H. Glavaš, L. Józsa, T. Barić, Infrared thermography in energy audit of electrical installations, *Tehnički vjesnik* 23 (5) (2016) 1533–1539.
- [46] C. Xu, N. Zhou, J. Xie, X. Gong, G. Chen, G. Song, Investigation on eddy current pulsed thermography to detect hidden cracks on corroded metal surface, *NDT & E International* 84 (2016) 27–35.
- [47] FLIR Camera Mounted, <https://www.thinkdefence.co.uk/2014/02/future-maritime-patrol-part-4-cheaper-options/flir-sensor-lg/>, [Online].
- [48] Controp, <https://www.laserfocusworld.com/articles/2016/07/controp-releases-lightweight-high-definition-eo-ir-camera-payload-for-helicopters.html>, [Online].
- [49] Yuneec Typhoon, <https://us.yuneec.com/typhoon-h-overview>, [Online].
- [50] FLIR Vehicle Lightweight Camera, <https://www.flir.eu/news-center/military/flir-lightweight-vehicle-surveillance-system-lvss/>, [Online].

- [51] HT Portable Camera, <https://www.ht-instruments.com/en/products/infrared-cameras/>, [Online].
- [52] R. Adhikari, E. Lucchi, V. Pracchi, Experimental Measurements on Thermal Transmittance of the Opaque Vertical Walls in the Historical Buildings Proceedings of PLEA2012. 28th Conference, Opportunities, Limits & Needs Towards An Environmentally Responsible Architecture (2012) 1248–1256.
- [53] P. Baker, U values and traditional buildings: in situ measurements and their comparisons to calculated values, Historic Scotland Technical Paper 10 (2011).
- [54] J. Bros Williamson, J. Stinson, C. Garnier, J. Currie, In situ monitoring of thermal refurbishment on pre 1919 properties in scotland, Int J Sustain Constr 2 (2014) 26–33.
- [55] C. rye, spab research report n.1: U value report, spab, london (2011).
- [56] I. Nardi, T. de Rubeis, M. Taddei, D. Ambrosini, S. Sfarra, The energy efficiency challenge for a historical building undergone to seismic and energy refurbishment, Energy Procedia 133 (2017) 231–242.
- [57] M. Jiménez, B. Porcar, M. Heras, Application of different dynamic analysis approaches to the estimation of the building component u value, Building and Environment 44 (2) (2009) 361–367.
- [58] A. H. Deconinck, S. Roels, Comparison of characterisation methods determining the thermal resistance of building components from onsite measurements, Energy and Buildings 130 (2016) 309–320.
- [59] E. Sassine, A practical method for in situ thermal characterization of walls, Case Studies in Thermal Engineering 8 (2016) 84–93.
- [60] K. Gaspar, M. Casals, M. Gangolells, In situ measurement of façades with a low u-value: Avoiding deviations, Energy and Buildings 170 (2018) 61–73.
- [61] F. Asdrubali, G. Baldinelli, F. Bianchi, A quantitative methodology to evaluate thermal bridges in buildings, Applied Energy 97 (2012) 365–373.
- [62] I. A. Atsonios, I. D. Mandilaras, D. A. Kontogeorgos, M. A. Founti, Two new methods for the in situ measurement of the overall thermal transmittance of cold frame lightweight steel framed walls, Energy and Buildings 170 (2018) 183–194.
- [63] R. ALBATICI, A. TONELLI, Verifica sperimentale in situ, con analisi termografiche e algoritmi di calcolo, della trasmittanza termica di un elemento costruttivo (), Museo Civico di Rovereto, Italy (2008) 103–125.

- [64] P. G. Cesaratto, M. De Carli, S. Marinetti, Effect of different parameters on the in situ thermal conductance evaluation, *Energy and buildings* 43 (7) (2011) 1792–1801.
- [65] G. Ficco, F. Iannetta, E. Ianniello, F. R. d. A. Alfano, M. Dell Isola, U value in situ measurement for energy diagnosis of existing buildings, *Energy and Buildings* 104 (2015) 108–121.
- [66] M. Scarpa, P. Ruggeri, F. Peron, M. Celebrin, M. De Bei, New measurement procedure for u value assessment via heat flow meter, *Energy Procedia* 113 (2017) 174–181.
- [67] Astm international (american society for testing and materials), standard test method for steady state heat flux measurements and thermal transmission properties by means of the guarded hot plate apparatus, designation c177, astm, west conshohocken (2013).
- [68] Iso (international organization for standardization), thermal insulation. determination of steady state thermal resistance and related properties. heat flow meter apparatus, standard iso 8301, iso, geneva (2014).
- [69] Ocana sm, guerrero ic, requena ig. thermographic survey of two rural buildings in spain. *energy and buildings.* (2004 Jun 1;36(6):515-23.).
- [70] T. Kobari, J. Okajima, A. Komiya, S. Maruyama, Development of guarded hot plate apparatus utilizing peltier module for precise thermal conductivity measurement of insulation materials, *International Journal of Heat and Mass Transfer* 91 (2015) 1157–1166.
- [71] R. Ricciu, L. A. Besalduch, A. Galatioto, G. Ciulla, Thermal characterization of insulating materials, *Renewable and Sustainable Energy Reviews* 82 (2018) 1765–1773.
- [72] C. S. Sanjaya, T. H. Wee, T. Tamilselvan, Regression analysis estimation of thermal conductivity using guarded hot plate apparatus, *Applied Thermal Engineering* 31 (10) (2011) 1566–1575.
- [73] J. Wang, C. Demartino, Y. Xiao, Y. Li, Thermal insulation performance of bamboo and wood based shear walls in light frame buildings, *Energy and Buildings* 168 (2018) 167–179.
- [74] J. Sala, A. Urresti, K. Martín, I. Flores, A. Apaolaza, Static and dynamic thermal characterisation of a hollow brick wall: Tests and numerical analysis, *Energy and Buildings* 40 (8) (2008) 1513–1520.
- [75] K. G. Wakili, C. Tanner, U-value of a dried wall made of perforated porous clay bricks: Hot box measurement versus numerical analysis, *Energy and Buildings* 35 (7) (2003) 675–680.
- [76] D. Aviram, A. Fried, J. Roberts, Thermal properties of a variable cavity wall, *Building and Environment* 36 (9) (2001) 1057–1072.

- [77] H. Kus, E. Özkan, Ö. Göcer, E. Edis, Hot box measurements of pumice aggregate concrete hollow block walls, *Construction and Building Materials* 38 (2013) 837–845.
- [78] E. H. Ridouane, M. Bianchi, Three dimensional numerical evaluation of thermal performance of uninsulated wall assemblies, Tech. rep., National Renewable Energy Lab.(NREL), Golden, CO (United States) (2011).
- [79] S. Ferrari, V. Zanotto, The thermal performance of walls under actual service conditions: Evaluating the results of climatic chamber tests, *Construction and Building Materials* 43 (2013) 309–316.
- [80] Y. Gao, J. Roux, C. Teodosiu, L. Zhao, Reduced linear state model of hollow blocks walls, validation using hot box measurements, *Energy and buildings* 36 (11) (2004) 1107–1115.
- [81] C. Ibarra Castanedo, J. R. Tarpani, X. P. Maldague, Nondestructive testing with thermography, *European Journal of Physics* 34 (6) (2013) S91.
- [82] C. pearson, thermal imaging of building fabric, bisra guide bg39, bisra, bracknell (2011).
- [83] I. Danielski, M. Froling, Diagnosis of buildings thermal performance a quantitative method using thermography under non steady state heat flow, *Energy Procedia* 83 (2015) 320–329.
- [84] E. Lucchi, Non invasive method for investigating energy and environmental performances in existing buildings, in: PLEA Conference on Passive and Low Energy Architecture, 2011.
- [85] G. Dall, E. Lucchi, G. Poliseno, Infrared scanning on buildings as a tool for evaluating pathologies and suggesting energy retrofit actions, in: 47th AiCARR International Conference on Systems, Energy and Built Environment toward a Sustainable Comfort, Tivoli, Roma, Italy, Vol. 89, 2009.
- [86] A. Thumann, W. J. Younger, *Handbook of energy audits*, The Fairmont Press, Inc., 2008.
- [87] B. M. Marino, N. Muñoz, L. P. Thomas, Estimation of the surface thermal resistances and heat loss by conduction using thermography, *Applied Thermal Engineering* 114 (2017) 1213–1221.
- [88] A. Rogalski, Infrared detectors: status and trends, *Progress in quantum electronics* 27 (2-3) (2003) 59–210.
- [89] J. P. Miller, N. Singh, Kinetic super resolution long wave infrared (ksr lwir) thermography diagnostic for building envelopes: Scott afb, il, Tech. rep., ENGINEER RESEARCH AND DEVELOPMENT CENTER CHAMPAIGN IL CONSTRUCTION (2015).
- [90] Essess thermal technology. (2017).
- [91] J. Armstrong, K. Butcher, J. Rowe, *CIBSE concise handbook*, Chartered Institution of Building Services Engineers, 2003.

- [92] A. Tibbs, Using infrared thermography to assess building problems, Cleveland, OH: Closer Look Inspections (2004).
- [93] J. Snell, M. Schwoegler, The use of infrared thermal imaging for home weatherization, The Snell Group (2012) 6.
- [94] Sagewell Inc., Cambridge, <http://https://www.sagewell.com/>, [Online].
- [95] Projected2perform, https://www.projected2perform.com/residential_thermal-imaging/, [Online].
- [96] SafetyHawaii, <http://www.safetywisehawaii.com/>, [Online].
- [97] K. Koiner, A. Rosener, D. Sadhukhan, D. F. Selvaraj, Z. E. Mrabet, M. Dunlevy, P. Ranganathan, Heat loss estimation using uas thermal imagery, in: IEEE EIT 2019, IEEE, 2019.
- [98] A. Donatelli, P. Aversa, V. A. M. Luprano, Set up of an experimental procedure for the measurement of thermal transmittances via infrared thermography on lab made prototype walls, *Infrared Physics & Technology* 79 (2016) 135–143.
- [99] J. Sun, Analysis of pulsed thermography methods for defect depth prediction, *Journal of Heat Transfer* 128 (4) (2006) 329–338.
- [100] A. Moropoulou, T. Tsiorva, K. Bisbikou, V. Tsantila, G. Biscontin, G. Longega, M. Groggia, E. Dalaklis, A. Petritaki, Evaluation of cleaning procedures on the facades of the bank of greece historical building in the center of athens, *Building and Environment* 37 (7) (2002) 753–760.
- [101] F. Luzi, M. Mitchell, C. Nanni, V. Redaelli, et al., Thermography: current status and advances in livestock animals and in veterinary medicine., *Thermography: current status and advances in livestock animals and in veterinary medicine.* (2013).
- [102] R. S. Adhikari, E. Lucchi, V. Pracchi, Experimental measurements on thermal transmittance of the opaque vertical walls in the historical buildings, in: Proceedings of PLEA2012. 28th Conference, Opportunities, Limits & Needs Towards an environmentally responsible architecture. Lima, 2012, pp. 1248–1256.
- [103] A. Muscio, P. G. Bison, S. Marinetti, E. Grinzato, Thermal diffusivity measurement in slabs using harmonic and one dimensional propagation of thermal waves, *International Journal of thermal sciences* 43 (5) (2004) 453–463.
- [104] P. Bison, S. Marinetti, A. Mazzoldi, E. Grinzato, C. Bressan, Cross comparison of thermal diffusivity measurements by thermal methods, *Infrared physics & technology* 43 (3-5) (2002) 127–132.

- [105] P. Bison, F. Cernuschi, E. Grinzato, In depth and in plane thermal diffusivity measurements of thermal barrier coatings by ir camera: evaluation of ageing, *International Journal of thermophysics* 29 (6) (2008) 2149–2161.
- [106] G. Ferrarini, P. Bison, A. Bortolin, G. Cadelano, Thermal response measurement of building insulating materials by infrared thermography, *Energy and Buildings* 133 (2016) 559–564.
- [107] P. Bison, G. Cadelano, E. Grinzato, Thermographic signal reconstruction with periodic temperature variation applied to moisture classification, *Quantitative InfraRed Thermography Journal* 8 (2) (2011) 221–238.
- [108] International Organization for Standardization (ISO). Thermal insulation. Qualitative detection of thermal irregularities in building envelopes. infrared method, standard iso 6781., Genève: ISO; 2010.
- [109] European Committee for Standardization (CEN). thermal performance of buildings. qualitative detection of thermal irregularities in building envelopes, infrared method, standard en 13187., Brussels: CEN; 1998.
- [110] T. I. Ward, G. Hannah, C. H. Sanders, Conventions for calculating linear thermal transmittance and temperature factors, IHS BRE Press, 2016.
- [111] T. I. Ward, Assessing the effects of thermal bridging at junctions and around openings, no. 1, 2006.
- [112] T. Taylor, J. Counsell, S. Gill, Combining thermography and computer simulation to identify and assess insulation defects in the construction of building façades, *Energy and Buildings* 76 (2014) 130–142.
- [113] A. Tavukçuoğlu, A. Düzgüneş, E. Caner Saltık, Ş. Demirci, Use of ir thermography for the assessment of surface water drainage problems in a historical building, ağızkarahan (aksaray), turkey, *NDT & E International* 38 (5) (2005) 402–410.
- [114] S. Ribarić, D. Marčetić, D. S. Vedrina, A knowledge based system for the non destructive diagnostics of façade isolation using the information fusion of visual and ir images, *Expert Systems with Applications* 36 (2) (2009) 3812–3823.
- [115] V. P. Vavilov, A pessimistic view of the energy auditing of building structures with the use of infrared thermography, *Russian Journal of Nondestructive Testing* 46 (12) (2010) 906–910.
- [116] E. Bauer, E. Pavon, E. Barreira, E. K. De Castro, Analysis of building facade defects using infrared thermography: Laboratory studies, *Journal of Building Engineering* 6 (2016) 93–104.

- [117] S. Bagavathiappan, B. Lahiri, T. Saravanan, J. Philip, T. Jayakumar, Infrared thermography for condition monitoring a review, *Infrared Physics & Technology* 60 (2013) 35–55.
- [118] T. Kalamees, Air tightness and air leakages of new lightweight single-family detached houses in estonia, *Building and environment* 42 (6) (2007) 2369–2377.
- [119] J. Hart, A practical guide to infra red thermography for building surveys, *Building Research Establishment*, 1991.
- [120] International organization for standardization (iso). thermal performance of renewable and sustainable energy reviews 82 (2018) 3077 30903089 buildings. determination of air permeability of buildings. fan pressurization method., Standard ISO 9972, Bruxelles: ISO; 2006.
- [121] R. Albatici, A. M. Tonelli, Infrared thermovision technique for the assessment of thermal transmittance value of opaque building elements on site, *Energy and Buildings* 42 (11) (2010) 2177–2183.
- [122] G. DallÓ, L. Sarto, A. Panza, et al., Infrared screening of residential buildings for energy audit purposes: results of a field test, *Energies* 6 (8) (2013) 3859–3878.
- [123] I. Nardi, S. Sfarrà, D. Ambrosini, Quantitative thermography for the estimation of the u value: state of the art and a case study, in: *Journal of Physics: Conference Series*, Vol. 547, IOP Publishing, 2014, p. 012016.
- [124] I. Nardi, D. Paoletti, D. Ambrosini, T. de Rubeis, S. Sfarrà, Validation of quantitative ir thermography for estimating the u value by a hot box apparatus, in: *Journal of Physics: Conference Series*, Vol. 655, IOP Publishing, 2015, p. 012006.
- [125] R. Albatici, A. M. Tonelli, M. Chiogna, A comprehensive experimental approach for the validation of quantitative infrared thermography in the evaluation of building thermal transmittance, *Applied energy* 141 (2015) 218–228.
- [126] R. Madding, Finding r values of stud frame constructed houses with ir thermography, *Proc. InfraMation 2008* (2008) 261–277.
- [127] Y. Ham, M. Golparvar Fard, 3d visualization of thermal resistance and condensation problems using infrared thermography for building energy diagnostics, *Visualization in Engineering* 2 (1) (2014) 12.
- [128] L. Ibos, J. P. Monchau, V. Feuillet, Y. Candau, A comparative study of in situ measurement methods of a building wall thermal resistance using infrared thermography, in: *Twelfth International*

Conference on Quality Control by Artificial Vision 2015, Vol. 9534, International Society for Optics and Photonics, 2015, p. 9534I.

- [129] C. Ghiaus, Experimental estimation of building energy performance by robust regression, *Energy and buildings* 38 (6) (2006) 582–587.
- [130] R. D. L. Vollaro, C. Guattari, L. Evangelisti, G. Battista, E. Carnielo, P. Gori, Building energy performance analysis: A case study, *Energy and Buildings* 87 (2015) 87–94.
- [131] J. Kim, J. Lee, J. Kim, C. Jang, H. Jeong, D. Song, Appropriate conditions for determining the temperature difference ratio via infrared camera, *Building services engineering research and technology* 37 (3) (2016) 272–287.
- [132] S. Kato, K. Kuroki, S. Hagihara, Method of in situ measurement of thermal insulation performance of building elements using infrared camera, in: 6th International Conference on Indoor Air Quality, Ventilation & Energy Conservation in Buildings IAQVEC, Vol. 2007, Citeseer, 2007.
- [133] E. Grinzato, P. Bison, G. Cadelano, F. Peron, R value estimation by local thermographic analysis, in: Thermosense XXXII, Vol. 7661, International Society for Optics and Photonics, 2010, p. 76610H.
- [134] J. Thouvenel, Find a modern and quick method to determine the u value and the thermal characteristics of a building envelope using an ir camera (2012).
- [135] Y. Ham, M. Golparvar Fard, Automated cost analysis of energy loss in existing buildings through thermographic inspections and cfd analysis, in: ISARC. Proceedings of the International Symposium on Automation and Robotics in Construction, Vol. 30, Vilnius Gediminas Technical University, Department of Construction Economics ..., 2013, p. 1.
- [136] K. Ohlsson, T. Olofsson, Quantitative infrared thermography imaging of the density of heat flow rate through a building element surface, *Applied energy* 134 (2014) 499–505.
- [137] I. Simões, N. Simões, A. Tadeu, J. Riachos, Laboratory assessment of thermal transmittance of homogeneous building elements using infrared thermography, in: Proceedings of the 12th International Conference on Quantitative InfraRed Thermography, Bordeaux, France, 2014, pp. 7–12.
- [138] V. Tzifa, G. Papadakos, A. Papadopoulou, V. Marinakis, J. Psarras, Uncertainty and method limitations in a short time measurement of the effective thermal transmittance on a building envelope using an infrared camera, *Int. J. Sustain. Energy* (2014) 1–19.
- [139] I. Nardi, D. Paoletti, D. Ambrosini, T. De Rubeis, S. Sfarra, U value assessment by infrared thermography: A comparison of different calculation methods in a guarded hot box, *Energy and Buildings* 122 (2016) 211–221.

- [140] B. Tejedor, M. Casals, M. Gangolells, X. Roca, Quantitative internal infrared thermography for determining in situ thermal behaviour of façades, *Energy and Buildings* 151 (2017) 187–197.
- [141] A. Marshall, J. Francou, R. Fitton, W. Swan, J. Owen, M. Benjaber, Variations in the u value measurement of a whole dwelling using infrared thermography under controlled conditions, *Buildings* 8 (3) (2018) 46.
- [142] T. Kisilewicz, A. Wrobel, Quantitative infrared wall inspection, in: Proceeding of 10th International Conference on Quantitative InfraRed Thermography, Quebec, du CAO, Les Eboulements, 2010, pp. 78–81.
- [143] I. Nardi, D. Ambrosini, D. Paoletti, S. Sfarra, Combining infrared thermography and numerical analysis for evaluating thermal bridges in buildings: a case study, *Int. J. Eng. Res. Afr.* 5 (2015) 67–76.
- [144] M. O'Grady, A. A. Lechowska, A. M. Harte, Quantification of heat losses through building envelope thermal bridges influenced by wind velocity using the outdoor infrared thermography technique, *Applied energy* 208 (2017) 1038–1052.
- [145] M. O'Grady, A. A. Lechowska, A. M. Harte, Infrared thermography technique as an in situ method of assessing heat loss through thermal bridging, *Energy and Buildings* 135 (2017) 20–32.
- [146] G. Baldinelli, F. Bianchi, A. Rotili, D. Costarelli, M. Seracini, G. Vinti, F. Asdrubali, L. Evangelisti, A model for the improvement of thermal bridges quantitative assessment by infrared thermography, *Applied energy* 211 (2018) 854–864.
- [147] C. Boué, S. Holé, Infrared thermography protocol for simple measurements of thermal diffusivity and conductivity, *Infrared Physics & Technology* 55 (4) (2012) 376–379.
- [148] S. Dudić, I. Ignjatović, D. Šešlija, V. Blagojević, M. Stojiljković, Leakage quantification of compressed air using ultrasound and infrared thermography, *Measurement* 45 (7) (2012) 1689–1694.
- [149] M. B. Dufour, D. Derome, R. Zmeureanu, Analysis of thermograms for the estimation of dimensions of cracks in building envelope, *Infrared Physics & Technology* 52 (2-3) (2009) 70–78.
- [150] G. Desogus, S. Mura, R. Ricciu, Comparing different approaches to in situ measurement of building components thermal resistance, *Energy and Buildings* 43 (10) (2011) 2613–2620.
- [151] T. Tiihonen, Stefan boltzmann radiation on non convex surfaces, *Mathematical methods in the applied sciences* 20 (1) (1997) 47–57.

- [152] R. Albatici, F. Passerini, A. M. Tonelli, S. Gialanella, Assessment of the thermal emissivity value of building materials using an infrared thermovision technique emissometer, *Energy and buildings* 66 (2013) 33–40.
- [153] S. J. Kim, S. W. Lee, Air cooling technology for electronic equipment, CRC press, 1996.
- [154] M. Gaši, B. Milovanović, S. Gumbarević, Infrared thermography for dynamic thermal transmittance determination, in: International Conference on Sustainable Materials, Systems and Structures (SMSS 2019) Energy Efficient Building Design and Legislation, 2019.
- [155] W. Chow, K. Chan, Parameterization study of the overall thermal-transfer value equation for buildings, *Applied Energy* 50 (3) (1995) 247–268.
- [156] T. P. Wutka, H. Bryan, Overview of standard 90.1, *ASHRAE Journal* 32 (2) (1990) 26–32.
- [157] W. Chow, P. C. Yu, Comment on the overall thermal transfer value (ottv) for building energy control, *Journal of architectural engineering* 4 (4) (1998) 149–154.
- [158] W. Chow, C. Philip, Controlling building energy use by overall thermal transfer value (ottv), *Energy* 25 (5) (2000) 463–478.
- [159] P.-b. B. E. Code, Electrical and mechanical services department, Government of Hong Kong Special Administrative Region (2007).
- [160] E. Sowell, Load calculations for 200,640 zones, *ASHRAE transactions* 94 (1988) 716–736.
- [161] E. Sowell, Classification of 200,640 parametric zones for cooling load calculations, *ASHRAE transactions* 94 (1988) 754–777.
- [162] S. M. Harris, Study to categorize walls and roofs on the basis of thermal response, Ph.D. thesis, Oklahoma State University (1988).
- [163] W. Sheng, L. Zhang, I. Ridley, The impact of minimum ottv legislation on building energy consumption, *Energy Policy* 136 (2020) 111075.
- [164] P. Tummu, S. Chirarattananon, V. D. Hien, P. Chaiwiwatworakul, P. Rakkwamsuk, Formulation of an ottv for walls of bedroom in thailand, *Applied Thermal Engineering* 113 (2017) 334–344.
- [165] Y.-H. Lin, K.-T. Tsai, M.-D. Lin, M.-D. Yang, Design optimization of office building envelope configurations for energy conservation, *Applied energy* 171 (2016) 336–346.
- [166] M.-D. Yang, M.-D. Lin, Y.-H. Lin, K.-T. Tsai, Multiobjective optimization design of green building envelope material using a non-dominated sorting genetic algorithm, *Applied Thermal Engineering* 111 (2017) 1255–1264.

- [167] J. Yu, L. Tian, X. Xu, J. Wang, Evaluation on energy and thermal performance for office building envelope in different climate zones of china, *Energy and Buildings* 86 (2015) 626–639.
- [168] S. Goel, R. A. Athalye, W. Wang, et al., Enhancements to ashrae standard 90.1 prototype building models, Tech. rep., Pacific Northwest National Lab.(PNNL), Richland, WA (United States) (2014).
- [169] A. Standard, Standard 90-1975, *Energy Conservation in New Building Design* (1975).
- [170] J. Lee, S. Kim, J. Kim, D. Song, H. Jeong, Thermal performance evaluation of low-income buildings based on indoor temperature performance, *Applied Energy* 221 (2018) 425–436.
- [171] A. Council, Energy efficiency building standards in japan, Acesso em março (2007).
- [172] S. Vidas, P. Moghadam, Heatwave: A handheld 3d thermography system for energy auditing, *Energy and Buildings* 66 (2013) 445–460.
- [173] G. Baldinelli, F. Bianchi, Windows thermal resistance: Infrared thermography aided comparative analysis among finite volumes simulations and experimental methods, *Applied energy* 136 (2014) 250–258.
- [174] K. Maroy, K. Carbonez, M. Steeman, N. Van Den Bossche, Assessing the thermal performance of insulating glass units with infrared thermography: Potential and limitations, *Energy and Buildings* 138 (2017) 175–192.
- [175] A. Krenzinger, A. de Andrade, Accurate outdoor glass thermographic thermometry applied to solar energy devices, *Solar Energy* 81 (8) (2007) 1025–1034.
- [176] F. Cerdeira, M. Vázquez, J. Collazo, E. Granada, Applicability of infrared thermography to the study of the behaviour of stone panels as building envelopes, *Energy and Buildings* 43 (8) (2011) 1845–1851.
- [177] C. Meola, Infrared thermography of masonry structures, *Infrared physics & technology* 49 (3) (2007) 228–233.
- [178] C. Meola, R. Di Maio, N. Roberti, G. M. Carlomagno, Application of infrared thermography and geophysical methods for defect detection in architectural structures, *Engineering Failure Analysis* 12 (6) (2005) 875–892.
- [179] F. Ascione, N. Bianco, R. F. De Masi, F. de Rossi, G. P. Vanoli, Simplified state space representation for evaluating thermal bridges in building: Modelling, application and validation of a methodology, *Applied Thermal Engineering* 61 (2) (2013) 344–354.

- [180] F. Bianchi, A. Pisello, G. Baldinelli, F. Asdrubali, Infrared thermography assessment of thermal bridges in building envelope: Experimental validation in a test room setup, *Sustainability* 6 (10) (2014) 7107–7120.
- [181] L. Zalewski, S. Lassue, D. Rousse, K. Boukhalfa, Experimental and numerical characterization of thermal bridges in prefabricated building walls, *Energy Conversion and Management* 51 (12) (2010) 2869–2877.
- [182] <https://www.wunderground.com/>.
- [183] <https://supervise.ly/>.
- [184] A. Verma, P. Singh, J. S. R. Alex, Modified convolutional neural network architecture analysis for facial emotion recognition, in: 2019 International Conference on Systems, Signals and Image Processing (IWSSIP), IEEE, 2019, pp. 169–173.
- [185] P. Bharati, A. Pramanik, Deep learning techniques—r-cnn to mask r-cnn: A survey, in: *Computational Intelligence in Pattern Recognition*, Springer, 2020, pp. 657–668.
- [186] Y. Yu, K. Zhang, L. Yang, D. Zhang, Fruit detection for strawberry harvesting robot in non-structural environment based on mask-rcnn, *Computers and Electronics in Agriculture* 163 (2019) 104846.
- [187] T. Rakha, A. Gorodetsky, Review of unmanned aerial system (uas) applications in the built environment: Towards automated building inspection procedures using drones, *Automation in Construction* 93 (2018) 252 – 264. doi:<https://doi.org/10.1016/j.autcon.2018.05.002>.
- URL <http://www.sciencedirect.com/science/article/pii/S0926580518300165>
- [188] M. H. Shariq, B. R. Hughes, Revolutionising building inspection techniques to meet large-scale energy demands: A review of the state-of-the-art, *Renewable and Sustainable Energy Reviews* 130 (2020) 109979.

Measurement Type

Passive

Coeval
building

Theoretical approach
(Data Sheets)

Finite element analysis
(CFD)

Active

HFM
Measurement

Laboratory
testing

IR Camera

Qualitative and Quantitative Methods

Global IRT

Aerial

Unmanned
aerial vehicles

Street drive

Walk through

Non IRT

HFM
Measurements

Laboratory
testing

Heating Source

HPT

SML-HT

Laser
Thermography

+

IRT
(or)
Non-IRT

Applications

Building evaluation

Thermal bridge
assessment

Moisture assessment

Insulation
evaluation

Air leakage
assessment



(a)



(b)



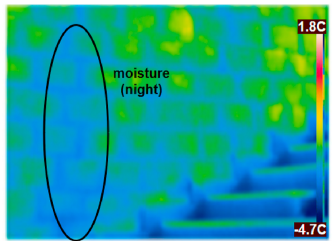
(c)



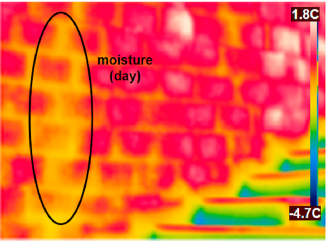
(d)



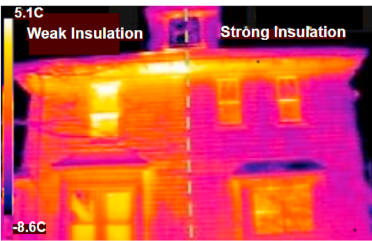
(e)



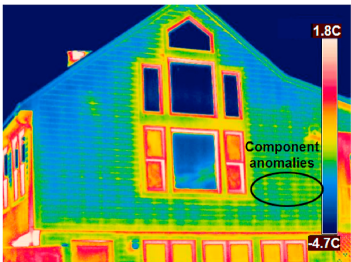
(a)



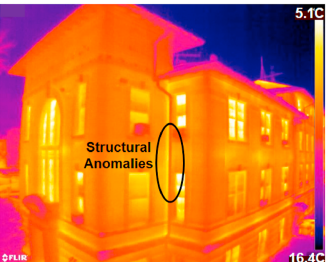
(b)



(c)



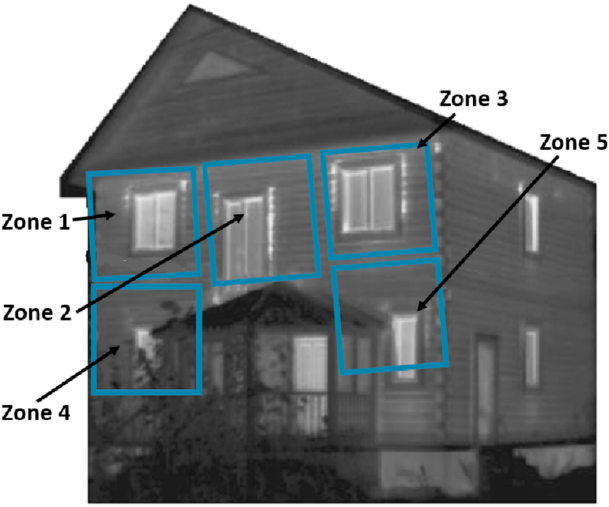
(d)



(e)



(f)



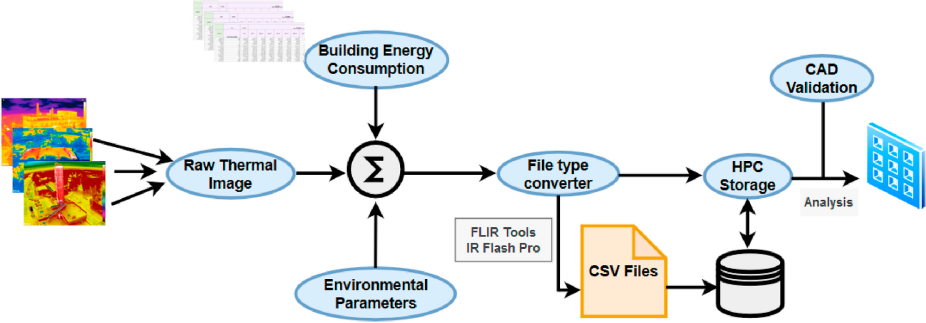
Zone 1

Zone 2

Zone 4

Zone 3

Zone 5



Database Layer



Image Data Repository

Preprocessing & Automation Layer

Background Elimination

Feature extraction

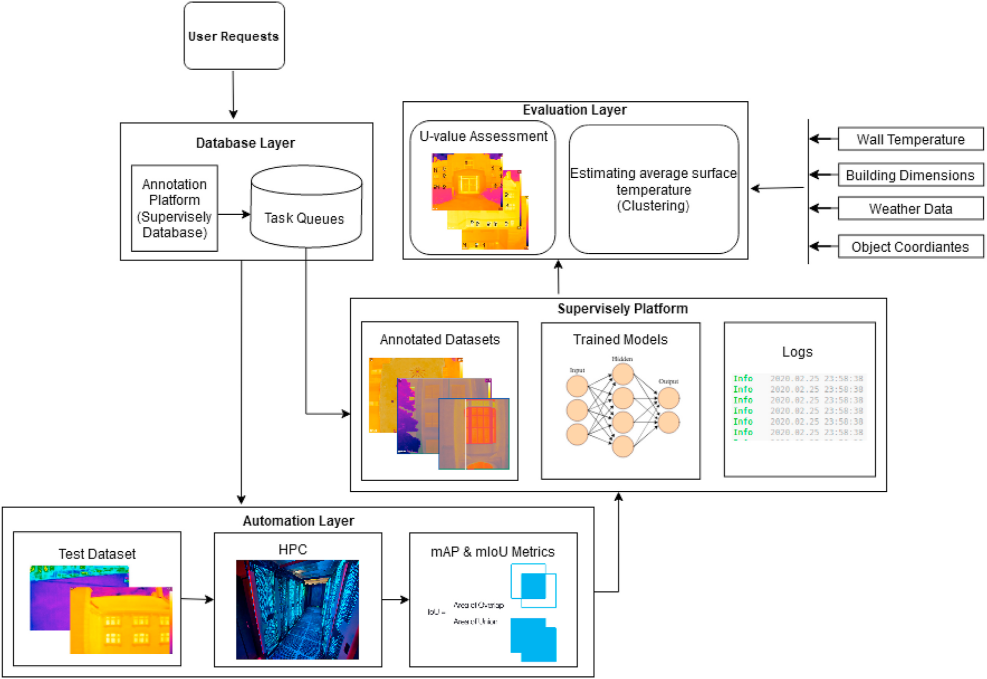
Instance Segmentation

Evaluation Layer

Heat Loss Estimation

Building element

Building envelope





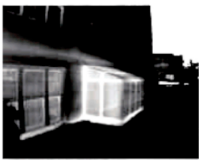
(a) Image 192
Edge detection



(b) Image 192
DCI



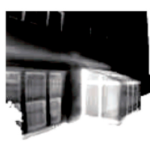
(c) Image 192
Ideal subtraction



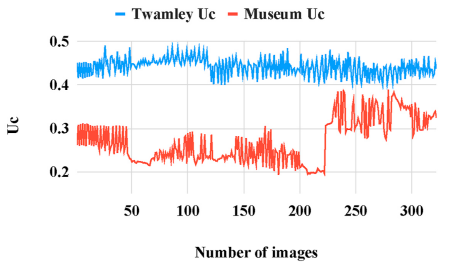
(d) Image 118
Edge detection



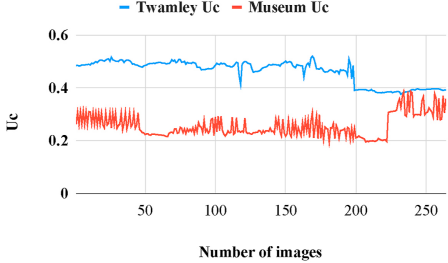
(e) Image 118
DCI



(f) Image 118
Ideal subtraction



(a) Single vs double pane window average U_c analysis

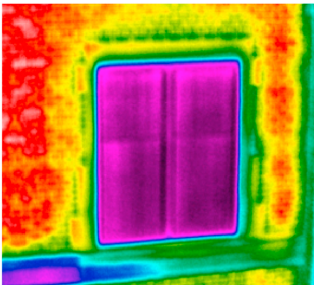


(b) Museum vs Twamley wall average wall U_c analysis

Raw Image



Thermal Image



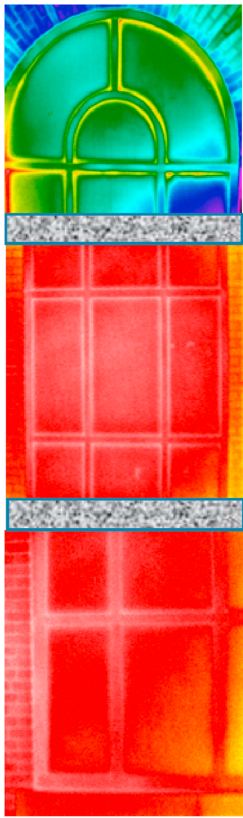
Average Temp: 14.55 C, U_c : 0.74 BTU/Ft²-hr-F

Single pane window

Raw Image



Thermal Image



Average Temp: 9.21 C, U-value: 0.18 BTU/Ft²-hr-F

Double pane window

Our paper provides:

- 1) A comprehensive review of thermal performance assessment techniques;
- 2) Guidelines on how to capture thermal data from UAS;
- 3) A novel three-layered ML framework to estimate building surface temperatures;
- 4) Potential solutions for future work

Conflict of Interest and Authorship Conformation Form

Please check the following as appropriate:

- ✓ All authors have participated in (a) conception and design, or analysis and interpretation of the data; (b) drafting the article or revising it critically for important intellectual content; and (c) approval of the final version.
- ✓ This manuscript has not been submitted to, nor is under review at, another journal or other publishing venue.
- ✓ The authors have no affiliation with any organization with a direct or indirect financial interest in the subject matter discussed in the manuscript
- ✓ The following authors have affiliations with organizations with direct or indirect financial interest in the subject matter discussed in the manuscript:

Author's name	Affiliation
Debanjan Sadhukhan	University of North Dakota
Sai Peri	University of North Dakota
Niroop Sugunaraj	University of North Dakota
Avhishek Biswas	University of North Dakota
Daisy Flora Selvaraj	University of North Dakota
Katelyn Koiner	University of North Dakota
Andrew Rosener	University of North Dakota
Matt Dunlevy	SkySkopes Inc, USA
Neena Goveas	BITS Pilani, Goa, India
David Flynn	University of North Dakota
Prakash Ranganathan	University of North Dakota

Declaration of competing interest

The authors would like to mention that there are no competing interests available.

Debanjan Sadhukhan, Sai Peri, Niroop Sugunaraj, Avhishek Biswas, Daisy Flora Selvaraj, Katelyn Koiner, Andrew Rosener, Matt Dunlevy, Neena Goveas, David Flynn, and Prakash Ranganathan